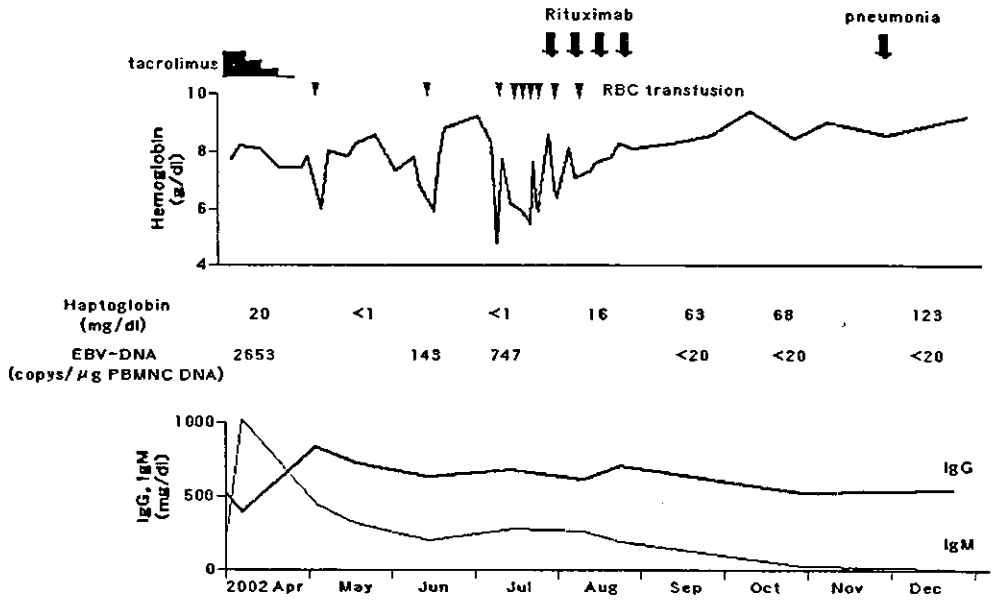

Fig. 1 Clinical course of the patient before and after rituximab treatment. *RBC* red blood cells, *EBV* Epstein-Barr Virus, *PBMNC* peripheral blood mononuclear cells, *Ig* immunoglobulin

were A-blood group and Rh-CcDEe groups. They were seropositive for EBV with no serological evidence of viral reactivation. As a graft-versus-host disease (GVHD) prophylaxis, a short-course methotrexate and cyclosporine A (CyA) were begun. Engraftment was rapid and PCR analysis of short tandem repeat polymorphism on peripheral blood leukocytes showed reconstitution with 100% donor cells on day 14. The hemoglobin level was 8–10 g/dl and platelet count 30–50×10^9/l without the need for blood transfusion. On day 90, chronic GVHD occurred, but was alleviated when the dose of CyA was increased. On day 150, chronic GVHD recurred while CyA decreased gradually. Tacrolimus 5 mg/day and prednisolone 40 mg/day were substituted for CyA. After symptoms of chronic GVHD improved, tacrolimus and prednisolone were slowly tapered.

In April 2002, 19 months after transplantation, the serum immunoglobulin M (IgM) level increased to 1,022 mg/dl, a time when the doses of tacrolimus and prednisolone were 1.5 mg/day and 10 mg/day, respectively. Immuno-electrophoresis analysis revealed monoclonality of IgM. There was a remarkable proliferation of EBV-DNA (2,653 copies/μg peripheral blood mononuclear cells DNA with a quantitive real-time PCR method) occurred, as shown in Fig. 1. Tacrolimus and prednisolone were rapidly tapered off because PTLD could become distinct. After that, the IgM level and EBV-DNA decreased but monoclonality of IgM remained. Hemoglobin levels became unstable about that time and she required red blood cell transfusion. In July 2002, severe anemia and hepato-splenomegaly occurred. Complete blood count showed a hemoglobin of 4.8 g/dl, reticulocyte count 96.4×10^9/l, WBC 5.3×10^9/l and platelets 34.0×10^9/l. Total and unconjugated bilirubin levels were increased (2.0 mg/dl and 1.5 mg/dl, respectively), lactate dehydrogenase (LDH) was also increased 600 U/l. Direct and indirect Coombs test were positive (direct Coombs test: +++, indirect Coombs test: +++). Red blood cell-associated IgG (RBC-IgG) was elevated to 477 molecules per one RBC (normal range; 20–46 molecules per one RBC). Antibody identification was anti-RhC+e antigen. PCR analysis of peripheral blood showed 100% donor chimerism. Bone marrow aspiration revealed erythroid hyperplasia and a diagnosis of AIHA was made. She required a blood transfusion twice or more per week to maintain the hemoglobin level above 6 g/dl. Due to the existence of predictive factors of PTLD, that was another increase in EBV-DNA and monoclonal gammopathy of IgM; conventional immunosuppressive therapy for AIHA was not considered to be a desirable option. We decided to give her rituximab, a mouse/human chimeric anti-CD20 antibody (Chugai Pharmaceutical, Tokyo, Japan), 375 mg/m^2 once weekly for a total of four doses. Prior to this treatment, she gave written informed consent. The drug was well tolerated and she had no adverse reactions. Clinical and laboratory signs of hemolysis rapidly improved and the hemoglobin level began to improve 2 weeks after the start of rituximab treatment. Both direct and indirect Coombs test became negative. EBV-DNA and monoclonal protein were undetectable using PCR and immuno-electrophoresis analysis, respectively. She developed acute pneumonia 4 months after start of the rituximab treatment, but recovered when put on intravenous immunoglobulin and antibiotics therapy. Now, at 10 months after the end of rituximab treatment, there has been no recurrence of hemolytic anemia or monoclonal gammopathy. EBV-DNA in peripheral blood mononuclear cells remains undetectable.

Discussion

The incidence of AIHA in patients who have undergone an allograft has been reported to be 3.1 to 5% [2, 3]. Although the exact mechanisms involved in post allogeneic transplant AIHA are poorly understood, post-transplant lymphoid regeneration is imperfect and defective regulation of autoreactive B cells can occur as a result of T cell defects, therefore causing an increase in autoimmune disorders. Reported cases of AIHA seem to occur exclusively in T-cell-depleted transplant cases and are concomitant with the development of GVHD [3], probably reflecting an increased defective T cell function in the face of GVHD and T cell depletion. Treatment of AIHA in these patients may be particularly difficult. Although immunosuppressive therapies can be effective for AIHA patients, the overall prognosis has been generally poor because of increase of complications related to infection. Immunosuppressive therapy was not productive in our patient probably because proliferation of EBV was evident. The relationship between EBV and AIHA in our patient is not clear. Proliferation of EBV and monoclonal gammopathy (IgM subclass) in our patient may be unrelated to development of AIHA directly because subclass of anti-RhC+e antigen was IgG.

PTLD is also a serious complication after transplantation. In a large series of PTLD, prolonged immunosuppression has been proposed to be a risk factor for the development of PTLD in transplant recipients [11, 15]. In our patient, the long-term immunosuppressive therapy for chronic GVHD was thought to be a cause of PTLD. Reduction of immunosuppressive agents is the first-line therapeutic approach for PTLD [10]. Adoptive immunotherapy using donor lymphocyte infusion (DLI) can also be an effective treatment for PTLD, but it was considered that chronic GVHD would get worse in our patient.

Recent studies have shown that rituximab, a highly specific mouse/human chimeric anti-CD20 antibody, is effective for some autoimmune disorders such as AIHA [7, 14], and rituximab has also been reported to be effective in PTLD [4, 5, 13]. Although the exact mechanism of action of rituximab in AIHA is unclear, several hypotheses have been proposed [12]. Elimination of CD20 expressing the pre-Ig heavy chain switched to plasmablasts and a small number of post-Ig heavy chain switched to plasma cells (possibly responsible for producing pathogenic auto-antibodies) following treatment with rituximab may partly explain the activity of rituximab in autoimmune disorders. Use of rituximab is attractive because it could reduce or avoid some adverse effects of prolonged immunosuppressive therapy.

Zecca et al. [14] and Hongeng et al. [7] proposed that two doses of rituximab might be sufficient for treatment of AIHA. We administered four doses of rituximab, because the patient was thought to be in a pre-PTLD status at the same time.

Depletion of B cells might make the patient more prone to some infections. Intravenous immunoglobulin may be needed as supportive therapy until there is sufficient evidence of regeneration of humoral immunity.

In conclusion, even though a longer follow-up is required to assess the long-term efficacy of this treatment, our experience deserves consideration in the treatment of post-allogeneic stem cell transplant patients with AIHA, especially in patients with problems for which immunosuppressive therapy is not feasible.

Acknowledgments We are grateful to S. Yoshida for performing quantitive real-time PCR assays of EBV, and to T. Kamesaki and E. Kajii for measuring red blood cell-associated IgG. We thank M. Kitayama and I. Sato for technical assistance.

References

1. Badley AD, Portela DF, Patel R, Kyle RA, Habermann TM, Strickler JG, Ilstrup DM, Wiesner RH, Groen P, Walker RC, Paya CV (1996) Development of monoclonal gammopathy precedes the development of Epstein-Barr lymphoproliferative disorder. Liver Transpl Surg 2:375–382
2. Chen FE, Owen I, Savage D, Roberts I, Apperley J, Goldman JM, Laffan M (1997) Late onset haemolysis and red cell autoimmunisation after allogeneic bone marrow transplant. Bone Marrow Transplant 19:491–495
3. Drobyski WR, Potluri J, Sauer D, Gottschall JL (1996) Autoimmune hemolytic anemia following T cell-depleted allogeneic bone marrow transplantation. Bone Marrow Transplant 17:1093–1099
4. van Esser JW, Niesters HGM, van der Holt B, Meijer E, Osterhaus ADME, Gratama JW, Verdonck LF, Lowenberg B, Cornelissen JJ (2002) Prevention of Epstein-Barr virus-lymphoproliferative disease by molecular monitoring and preemptive rituximab in high-risk patients after allogeneic stem cell transplantation. Blood 99:4364–4369
5. Faye A, Quartier P, Reguerre Y, Lutz P, Carret AS, Dehee A, Rohrlich P, Peuchmaur M, Matthieu-Boue A, Fischer A, Vilmer E (2001) Chimeric anti-CD20 monoclonal antibody (rituximab) in post-transplant B-lymphoproliferative disorder following stem cell transplantation in children. Br J Haematol 115:112–118
6. Fischer A, Landais P, Friedrich W, Gerritsen B, Fasth A, Porta F, Vellodi A, Benkerrou M, Jais JP, Cavazzana-Calvo M, et al (1994) Bone marrow transplantation in Europe for primary immunodeficiencies other than severe combined immunodeficiency ESCT/EGID report. Blood 83:1149–1154
7. Hongeng S, Tardtong P, Worapongpaiboon S, Ungkanont A, Jootar S (2002) Successful treatment of refractory autoimmune haemolytic anaemia in a post-unrelated bone marrow transplant paediatric patient with rituximab. Bone Marrow Transplant 29:871–872
8. Horn B, Viele M, Mentzer W, Mogck N, DeSantes K, Cowan M (1999) Autoimmune hemolytic anemia in patients with SCID after T cell-depleted BM and PBSC transplantation. Bone Marrow Transplant 24:1009–1013
9. Nishio M, Nakao S, Endo T, Fujimoto K, Takashima H, Sakai T, Bacigalupo A, Koike T, Sawada K (2001) Successful nonmyeloablative stem cell transplantation for a heavily transfused woman with severe aplastic anemia complicated by heart failure. Bone Marrow Transplant 28:783–785
10. Paya CV, Fung JJ, Nalesnik MA, Kieff E, Green M, Gores G, Habermann TM, Wiesner PH, Swinnen JL, Woodle ES, Bromberg JS (1999) Epstein-Barr virus-induced post-transplant lymphoproliferative disorders. ASTS/ASTP EBV-PTLD Task Force and The Mayo Clinic Organized International Consensus Development Meeting. Transplantation 68:1517–1525
11. Shapiro RS, McClain K, Frizzera G, Gajl-Peczalska KJ, Kersey JH, Blazar BR, Arthur DC, Patton DF, Greenberg JS, Burke B, et al (1988) Epstein-Barr virus associated B cell lymphoproliferative disorders following bone marrow transplantation. Blood 71:1234–1243
12. Treon SP, Anderson KC (2000) The use of rituximab in the treatment of malignant and non malignant plasma cell disorders. Semin Oncol 27:79–85
13. Verschuuren EA, Stevens SJ, van Imhoff GW, Middeldorp JM, de Boer C, Koeter G, The TH, van Der Bij W (2002) Treatment of posttransplant lymphoproliferative disease with rituximab: the remission, the relapse, and the complication. Transplantation 73:100–104
14. Zecca M, De Stefano P, Nobili B, Locatelli F (2001) Anti-CD20 monoclonal antibody for the treatment of severe, immunemediated pure red cell aplasia and hemolytic anemia. Blood 97:3995–3997
15. Zutter MM, Martin PJ, Sale GE, Shulman HM, Fisher L, Thomas ED, Durnam DM (1988) Epstein-Barr virus lymphoproliferation after bone marrow transplantation. Blood 72:520–529

Eur J Haematol 2004: 72: 140–144
Printed in UK. All rights reserved

Copyright © Blackwell Munksgaard 2004

EUROPEAN
JOURNAL OF HAEMATOLOGY

Case report

Effective high-dose chemotherapy combined with CD34$^+$-selected peripheral blood stem cell transplantation in a patient with cutaneous involvement of nasal NK/T-cell lymphoma

Koizumi K, Fujimoto K, Haseyama Y, Endo T, Nishio M, Yokota K, Itoh T, Sawada K, Koike T. Effective high-dose chemotherapy combined with CD34$^+$-selected peripheral blood stem cell transplantation in a patient with cutaneous involvement of nasal NK/T-cell lymphoma.
Eur J Haematol 2004: 72: 140–144. © Blackwelll Munksgaard 2004.

Abstract: The prognosis of nasal natural killer (NK)/T-cell lymphoma with cutaneous involvement especially is morbid despite intensive chemotherapy and radiotherapy. We treated a 52-yr-old Japanese woman with cutaneous dissemination of nasal NK/T-cell lymphoma. Six cycles of chemotherapy, irradiation to skin lesion were administered and complete remission (CR) was attained. High-dose chemotherapy (HDC; etoposide 750 mg/m^2 × 2 d, cyclophosphamide 60 mg/kg × 2 d, total body irradiation 12 Gy two daily fractions × 3 d) followed by CD34$^+$-selected autologous peripheral blood stem cell transplantation (CD34$^+$-APBSCT) was then prescribed. Complete remission (CR) was obtained and she has been free of disease for 34 months since CD34$^+$-APBSCT. We suggest that marrow-ablative chemotherapy facilitated by autologous stem cell transplantation should be considered part of the primary therapy for subjects with a poor prognosis for nasal NK/T-cell lymphoma with cutaneous involvement.

Kazuki Koizumi[1], Katsuya Fujimoto[1], Yoshihito Haseyama[1], Tomoyuki Endo[1], Mitsufumi Nishio[1], Kouichi Yokota[2], Tomoo Itoh[3], Ken-ichi Sawada[4], Takao Koike[1]

Departments of [1]Internal Medicine II and [2]Dermatology, Hokkaido University School of Medicine, Sapporo, Hokkaido, Japan; [3]Department of Surgical Pathology, Hokkaido University Hospital, Sapporo, Hokkaido, Japan; [4]Department of Internal Medicine III, Akita University School of Medicine, Akita, Japan

Key words: nasal NK/T-cell lymphoma; CD34$^+$-selected APBSCT; high-dose chemotherapy; transplantation

Correspondence: Dr Kazuki Koizumi, Department of Internal Medicine II, Hokkaido University School of Medicine, N-15, W-7, Sapporo, Hokkaido 060-8638, Japan
Tel: 81-11-716-1161 (ext. 5916)
Fax: 81-11-706-7710
e-mail: koizumi@med.hokudai.ac.jp (or) taiki-k@zg7.so-net.ne.jp

Accepted for publication 22 August 2003

Nasal natural killer (NK)/T-cell lymphoma, a distinct clinicopathologic entity is characterized by its prevalence in East Asian countries. The NK-cell origin is evidenced by the expression of CD56 antigen without T-cell receptor (TCR) gene rearrangement and the expression of surface CD3 antigen, and by its almost exclusively extranodal occurrence (1). This lymphoma usually presents with localized extranodal disease, and radiotherapy and chemotherapy have been the most prescribed treatments. However, cases of widespread lesions show a highly aggressive course and resistance to ordinary anti-cancer chemotherapies can occur. NK/T-cell lymphoma with cutaneous involvement led to an aggressive course and a very poor outcome despite chemotherapy and radiotherapy (2–7). We report here our experience with a patient with cutaneous dissemination of nasal NK/T-cell lymphoma who was effectively treated with high-dose chemotherapy (HDC) followed by CD34$^+$-autologous peripheral blood stem cell transplantation (APBSCT).

Case report

A 52-yr-old Japanese woman herself detected a thumb-sized, red nodular lesion on her left hip in February 2000. Subsequently, similar multiple nodules appeared on her left forearm and on her lower extremities. On admission to the Hospital of

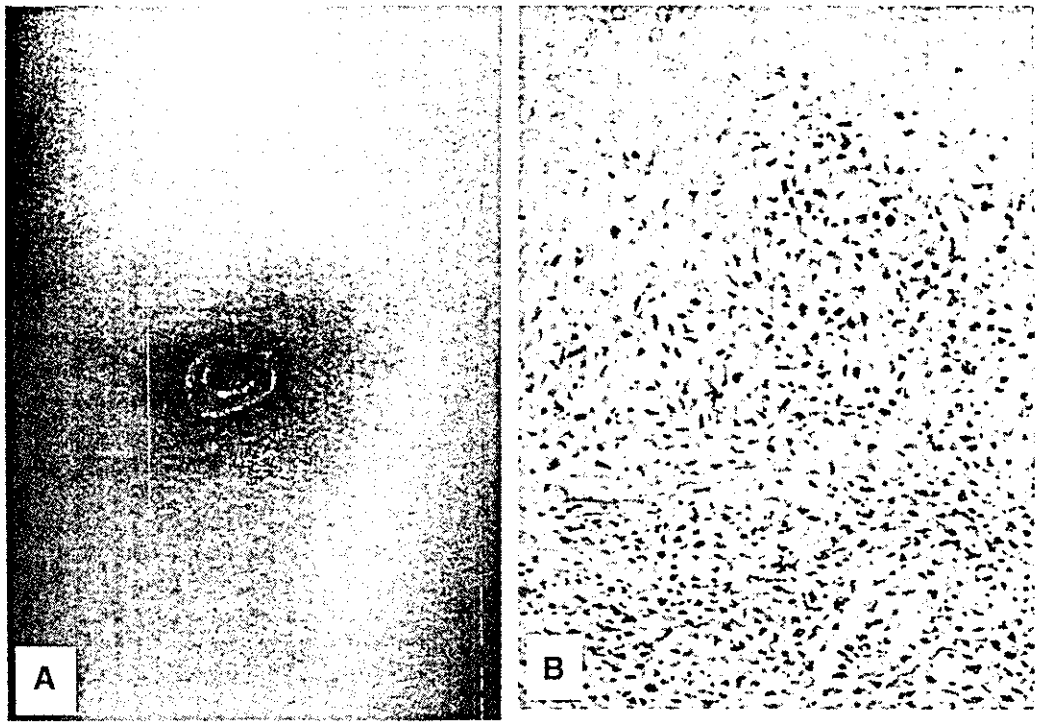

Fig. 1. (A) Subcutaneous tumor with extensive ulceration occurred on the left forearm. (B) Intermediated and large-sized atypical lymphocytes infiltrated from the upper dermis to the subcutaneous tissue (hematoxylin and eosin stain, ×20).

Hokkaido University School of Medicine in June 2000, there were multiple cutaneous nodules, some with ulceration, on her left hip, left forearm (Fig. 1A) and bilateral lower extremities. Systemic B symptoms were absent and vital signs were normal. She felt some nasal obstruction. Physical examination revealed a mass in the left nasal cavity. CT scan of the chest and abdomen revealed no evidence of peripheral lymphadenopathy and hepatosplenomegaly. Serum lactate dehydrogenase (LDH) was elevated to 591 IU/L (normal 200–460 IU/L), but other laboratory data were normal, including soluble interleukin-2 receptor (sIL-2R). Serologic studies were negative for human T-cell leukemia virus type I (HTLV-I) and human immunodeficiency virus (HIV). Serologic test for Epstein–Barr virus (EBV) antibodies showed the following titers: EBV viral capsid antigen (VCA) IgG 1 : 320, IgM less than 1 : 10, and IgA less than 1 : 20; EBV early antigen (EA) IgG less than 1 : 20 and IgA less than 1 : 10; and EB nuclear antigen (EBNA) 1 : 10. Bone marrow aspiration and biopsy revealed no involvement by atypical lymphocytes. The histology of the nasal tumor revealed proliferation of atypical lymphocytes with irregularly contoured nuclei, and immunohistochemical staining revealed that the tumor cells were positive for CD3, CD30, CD56 and cutaneous lymphocyte antigen (CLA) but negative for CD5 and CD20 (Fig. 2). EBV-encoded small RNAs (EBERs) were detected in tumor cells using *in situ* hybridization. Clonal gene rearrangement of T-cell receptor (TCR) was negative in the Southern blot analysis. Skin biopsy of a nodule on her left forearm showed angiocentric, angiodestructive proliferation of atypical lymphoid cells from the upper dermis to subcutaneous tissues (Fig. 1B). Clinical and histologic findings led to a diagnosis of extranodal NK/T-cell lymphoma, nasal type as described by the World Health Organization Classification of Tumors (WHO classification) (8). Her clinical stage was determined as IV A according to the Ann Arbor staging system. Her lymphoma was classified as high risk according to the International Prognostic Index (IPI), and as high-intermediate risk according to age-adjusted IPI (9). As the clinical course of NK/T-cell lymphoma with cutaneous involvement is aggressive and morbid despite intensive chemotherapy and radiotherapy, we prescribed intensive treatment with HDC followed by APBSCT, as first-line therapy. The patient was given three cycles of doxorubicin 50 mg/m^2 starting once daily i.v. on day 1, cyclophosphamide 750 mg/m^2 starting once daily i.v. on day 1, vincristine 2 mg starting once daily i.v. on day 1 and prednisolone 50 mg/m^2 p.o. in divided doses daily for 5 d (CHOP regimen) but the cutaneous lymphoma lesions remained. Therefore, purging of peripheral blood stem cells (PBSC) with CD34$^+$ cell selection was planned because we considered the likelihood

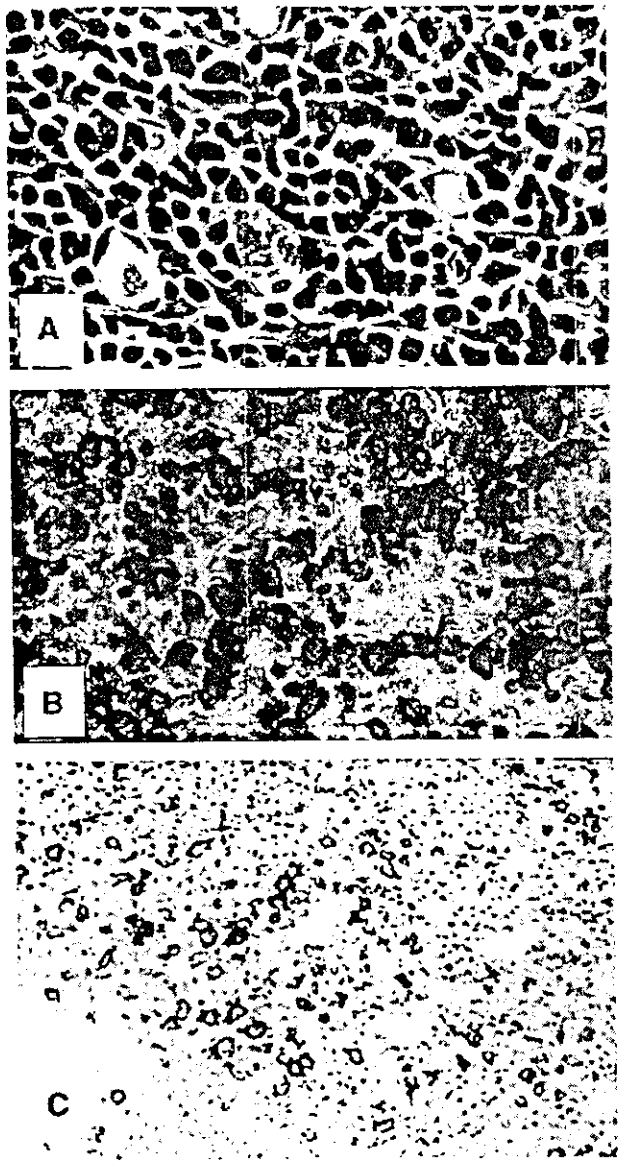

Fig. 2. (A) A higher magnification shows hyperchromatic and irregularly contoured nuclei of atypical lymphocytes infiltrating the nasal tumor (hematoxylin and eosin stain, ×100). (B) Infiltrating atypical lymphocytes are positive for CD56 (immunohistochemical staining of CD56, ×100). (C) Infiltrating atypical lymphocytes are positive for cutaneous lymphocyte antigen (CLA) (immunohistochemical staining of CLA, ×40).

of contamination by malignant cells based on our experience and related documentation (10,11). During hematopoietic recovery after the fourth course of CHOP therapy, PBSC were harvested by continuous leukapheresis. $CD34^+$ cells were positively immunoselected as described (12). This treatment of $CD34^+$-APBSCT was approved by the Ethical Committee in the Hokkaido University School of Medicine, and written informed consent was obtained from this patient. The overall purity of the $CD34^+$ cells was 98.0%. The proportion of $CD56^+$ cells was reduced from 0.50% to 0.08%. The purified $CD34^+$ cells and CFU-GM numbered 5.9×10^6 and 5.8×10^5/kg, respectively. During fifth and sixth cycles of CHOP therapy, she was given a total of 30 Gy of electron beam radiotherapy to cutaneous lesions and complete remission (CR) followed. After this therapy, $CD34^+$ APBSCT was initiated. The conditioning regimen given was etoposide 750 mg/m^2 once daily i.v. on day −7 and −6 and cyclophosphamide 60 mg/kg once daily i.v. on day −5 and −4 and total body irradiation 12 Gy two daily fractions from day −3 to day −1. This was started on 26 October 2000, and all purified $CD34^+$ cells were re-infused on 2 November 2000 (day 0). Cells infused included 5.9×10^6/kg $CD34^+$ cells, 5.8×10^5/kg CFU-GM and G-CSF.(5 μg/kg s.c.), administered from day 1 until the time of granulocyte recovery. After PBSCT, the time required to recover neutrophils over 0.5×10^9/l and platelets over 50×10^9/l was 8 and 29 d, respectively. As consolidation therapy, field radiotherapy (total 40 Gy) to the primary nasal site was given 7 wk after the PBSCT. She was discharged at the end of February 2001 and she remains in CR 34 months after $CD34^+$-APBSCT. Maintenance chemotherapy has not been given.

Discussion

Nasal NK/T-cell lymphomas, previously referred to as a lethal midline granuloma, follow an aggressive course and have a morbid prognosis. Clinically, the early stage cases (I and II) are confined to a single region and treated by irradiation therapy, with a rather favorable prognosis. However, cases of advanced disease show a highly aggressive course, as there is resistance to ordinary anti-cancer chemotherapy and radiotherapy. Cheung *et al.* (13) reported that the 2-yr disease-free survival (DFS) and overall survival (OS) rates were 13.3% and 20.0% in cases of stage IV. Cutaneous involvement is an important prognostic factor for patients with this lymphoma (7). We reviewed 26 cases of nasal NK/T-cell lymphoma with cutaneous involvement (Table 1) (2–7, 14, 15). Twenty-four were given standard chemotherapy and radiotherapy, 20 patients died several months after onset of the disease, one patient died after 36 months, one is alive after 5 months and the other two patients were alive but had a relapse. However, two patients, who received myeloablative chemotherapy with APBSCT, obtained CR and have been free of disease for 15 and 36 months (14, 15). Yoshino *et al.* (7) reported that most patients with nasal NK/T-cell lymphoma with cutaneous involvement (all of whom expressed CLA), had a poor prognosis, even

Table 1. Reported cases of nasal NK/T-cell lymphoma with skin involvement

Case	Age	Sex	Treatment	Outcome	Reference
1	56	M	CT	Dead, 8 months	2
2	69	F	CT, RT	Dead, 11 months	2
3	27	F	CT	Dead, 5 months	2
4	58	F	CT	Dead, 4 months	2
5	73	F	CT, RT	Dead, 7 months	3
6	44	M	CT	Dead, 11 months	3
7	19	F	CT, RT	Dead, 11 months	3
8	47	M	CT	Alive on disease, 29 months	4
9	74	M	CT	Alive on disease, 11 months	4
10	44	F	CT	Dead, 15 months	4
11	34	F	CT	Dead, 3 months	4
12	32	M	CT, RT	Dead, 17 months	5
13	70	M	CT	Dead, 4 months	6
14	38	F	CT, RT, APBSCT	Alive on CR, 36 months	14
15	54	F	CT, RT, APBSCT	Alive on CR, 15 months	15
16–24	ND	ND	CT and/or RT	Dead, within 12 months	7
25	ND	ND	CT and/or RT	Dead, 36 months	7
26	ND	ND	CT and/or RT	Alive, 5 months	7

M, male; F, female; CT, chemotherapy; RT, radiotherapy; APBSCT, autologous peripheral blood stem cell transplantation; CR, complete remission; ND, no data.

when only non-cutaneous cases were considered, hence the survival rate of the CLA-positive patients was significantly worse than that of the CLA-negative patients. This finding indicated the possibility of an undetectable level of distant skin involvement in non-cutaneous CLA^+ cases (7). As tumor cells in our patient were positive for CLA, her prognosis was considered to be morbid.

Several reports indicated that the efficacy of CHOP for nasal NK/T-cell lymphoma is inadequate even in localized cases, because disease progression frequently occurred early during CHOP chemotherapy (13, 16, 17). In this case the CHOP regimen was not completely effective, because the cutaneous lymphoma lesions remained after four courses of this regimen. Therefore electron beam radiotherapy to cutaneous lesions was given concurrently with fifth and sixth cycles of CHOP therapy, and CR was achieved. She received HDC immediately after she obtained CR. We are convinced that this systematic therapy schedule, including HDC, led to the good result. Yamaguchi *et al.* (18) reported the frequent expression of P-glycoprotein on nasal NK/T-cell lymphoma cells, which is the product of the multi-drug resistance (MRD) 1 gene. They proposed that DeVIC therapy, which consists of carboplatin, etoposide, ifosfamide and dexamethasone, is an effective therapy for nasal NK/T-cell lymphoma, because carboplatin and ifosfamide are multi-MRD-unrelated anticancer agents. Therefore, we recently use DeVIC therapy instead of CHOP therapy for treatment of this lymphoma.

We reported early and disseminated recurrence of cutaneous T-cell lymphoma and treated this patient with HDC followed by unpurged APBSCT (11). In this report, the form of recurrence suggested the possibility of contamination by malignant cells in PBSC (11). The positive selection of $CD34^+$ cells was reported to result in a 1–4 log reduction of tumor cells in apheresis products and a successful result of this procedure against poor prognosis hematologic malignancy has already been reported (19). We strongly worried about tumor cells contamination in PBSC products, because skin 'tumors in our patient remained at PBSC apheresis. On this basis we prescribed $CD34^+$-APBSCT. In our patient, PCR analysis could not be made but the frequency of $CD56^+$ cells, which was expressed in her tumor cells decreased from 0.50% to 0.08%. Although it cannot be ruled out that CR could have been attained with standard PBSCT, we were convinced that a considerable number of tumor cells in her apheresis products could be purged and $CD34^+$-APBSCT was effective for our patient. Because recurrence and a poor prognosis can occur after a short period in most cases, we decided that further additional therapy was necessary.

While it is difficult to determine the necessity and efficacy of $CD34^+$-APBSCT from such a small number of cases, it is strongly suggested that myeloablative chemotherapy followed by APBSCT may be effective for refractory cutaneous involvement cases of nasal NK/T-cell lymphoma in this and other reports (14, 15). Further follow-up and additional cases are needed to determine the overall efficacy of APBSCT for this type of nasal NK/T-cell lymphoma.

Acknowledgements

We thank M. Ohara (Fukuoka, Japan) for language assistance, J. Moriya and I. Sato for technical services.

References

1. Chan JK, Sin VC, Wong KF, Ng CS, Tsang WY, Chan CH, Cheung MM, Lau WH. Nonnasal lymphoma expressing the natural killer cell marker CD56: a clinicopathologic study of 49 cases of an uncommon aggressive neoplasm. Blood 1997;**89**:4501–4513.
2. Ahn SJ, Jang KA, Choi JH, Sung KJ, Moon KC, Koh JK. Nasal and nasal type CD56+ natural killer cell/T-cell lymphoma: a case with rapid progression to bone marrow involvement. Br J Dermatol 2000;**142**:1021–1025.
3. Chang SE, Lee SY, Choi JH, Sung KJ, Moon KC, Koh J. Cutaneous dissemination of nasal NK/T-cell lymphoma with bone marrow, liver and lung involvement. Clin Exp Dermatol 2002;**27**:120–122.
4. Hirakawa S, Kuyama M, Takahashi S *et al.* Nasal and nasal-type natural killer/T-cell lymphoma. J Am Acad Dermatol 1999;**40**:268–272.
5. Kato N, Yasukawa K, Onozuka T, Kikuta H. Nasal and nasal-type T/NK-cell lymphoma with cutaneous involvement. J Am Acad Dermatol 1999;**40**:850–856.

6. Miyamoto T, Yoshino T, Takehisa T, Hagari Y, Mihara M. Cutaneous presentation of nasal/nasal type T/NK cell lymphoma: clinicopathological findings of four cases. Br J Dermatol 1998;**139**:481–487.
7. Yoshino T, Nakamura S, Suzumiya J *et al.* Expression of cutaneous lymphocyte antigen is associated with a poor outcome of nasal-type natural killer-cell lymphoma. Br J Haematol 2002;**118**:482–487.
8. Harris NL, Jaffe ES, Diebold J, Flandrin G, Muller-Hermelink HK, Vardiman J, Lister TA, Bloomfield CD. The World Health Organization classification of hematological malignancies report of the Clinical Advisory Committee Meeting, Airlie House, Virginia, November 1997. Mod Pathol 2000;**13**:193–207.
9. The International Non-Hodgkin's Lymphoma Prognostic Factors Project A predictive model for aggressive non-Hodgkin's lymphoma. N Engl J Med 1993;**329**:987–994.
10. Muche JM, Lukowsky A, Asadullah K, Gellrich S, Sterry W. Demonstration of frequent occurrence of clonal T cell in the peripheral blood of patients with primary cutaneous T cell lymphoma. Blood 1997;**90**:1636–1642.
11. Nishio M, Sawada K, Koizumi K *et al.* Recurrence with histological transformation 40 days after autologous peripheral blood stem cell transplantation (APBSCT) for cutaneous CD30-negative large T cell lymphoma. Bone Marrow Transplant 1998;**22**:1211–1214.
12. Koizumi K, Nishio M, Endo T *et al.* Large scale purification of human blood CD34+ cells from cryopreserved peripheral blood stem cells, using a nylon-fiber syringe system and immunomagnetic microspheres. Bone Marrow Transplant 2000;**26**:787–793.
13. Cheung MM, Chan JK, Lau WH, Foo W, Chan PT, Ng CS, Ngan RK. Primary non-Hodgkin's lymphoma of the nose and nasopharynx: clinical features, tumor immunophenotype, and treatment outcome in 113 patients. J Clin Oncol 1998;**16**:70–77.
14. Sasaki M, Matsue K, Takeuchi M, Mitome M, Hirose Y. Successful treatment of disseminated nasal NK/T-cell lymphoma using double autologous peripheral blood stem cell transplantation. Int J Hematol 2000;**71**:75–78.
15. Sanda T, Lida S, Ito M, Tsuboi K, Miura K, Harada S, Komatsu H, Wakita A, Inagaki H, Ueda R. Successful treatment of nasal T-cell lymphoma with a combination of local irradiation and high-dose chemotherapy. Int J Hematol 2002;**75**:195–200.
16. Kwong YL, Chan AC, Liang R, Chiang AK, Chim CS, Chan TK, Todd D, Ho FC. CD56+ NK lymphomas: clinicopathological features and prognosis. Br J Haematol 1997;**97**:821–829.
17. Kim WS, Song SY, Ahn YC *et al.* CHOP followed by involved field radiation: is it optimal for localized nasal natural killer/T-cell lymphoma? Ann Oncol 2001;**12**:349–352.
18. Yamaguchi M, Ogawa S, Nomoto Y, Oka K, Taniguchi M, Nakase K, Kobayashi T, Shiku H. Treatment outcome of nasal NK-cell lymphoma: a report of 12 consecutively-diagnosed cases and a review of the literature. J Clin Exp Hematopathol 2001;**41**:93–99.
19. Nishio M, Koizumi K, Endo T, Takashima H, Haseyama Y, Fujimoto K, Yamamoto S, Kobayashi H, Koike T, Sawada K. Effective high-dose chemotherapy combined with CD34+-selected autologous peripheral blood stem cell transplantation in a patient with cutaneous CD30-negative large T cell lymphoma. Bone Marrow Transplant 2000;**25**:1315–1317.

0013-7227/04/$15.00/0
Printed in U.S.A.

Endocrinology 145(5):2346–2356
Copyright © 2004 by The Endocrine Society
doi: 10.1210/en.2003-1180

Identification of a Functional Peroxisome Proliferator-Activated Receptor Responsive Element within the Murine Perilipin Gene

SO NAGAI, CHIKARA SHIMIZU, MASAAKI UMETSU, SATOSHI TANIGUCHI, MIKIKO ENDO, HIDEAKI MIYOSHI, NARIHITO YOSHIOKA, MITSUMASA KUBO, AND TAKAO KOIKE

Department of Medicine II (S.N., C.S., M.U., S.T., M.E., H.M., N.Y., T.K.), Hokkaido University Graduate School of Medicine, Sapporo 060-8638, Japan; and Health Administration Center, Hokkaido University of Education (M.K.), Sapporo 002-8501, Japan

Perilipin, a family of phosphoproteins located around lipid droplets in adipocytes, is essential for enlargement of lipid droplets and lipolytic reaction by hormone-sensitive lipase. Thiazolidinediones, peroxisome proliferator-activated receptor (PPAR) γ agonists, have been shown to increase perilipin expression in fully differentiated adipocytes. However, the precise mechanism of transcriptional regulation of murine perilipin gene heretofore remains unclear. We determined the transcription start site of murine perilipin gene by RNA ligase-mediated rapid amplification of the cDNA ends method. We generated luciferase reporter gene constructs containing various lengths of the 5′-flanking region of the murine perilipin gene and assayed promoter/enhancer activities using differentiated 3T3-L1 adipocytes. We identified a functional PPAR-responsive element (PPRE) in the murine perilipin promoter, and this was confirmed by gel EMSAs using nuclear extracts from differentiated 3T3-L1 adipocytes. Furthermore, point mutations of the identified functional PPRE markedly reduced both the reporter gene activity in differentiated 3T3-L1 adipocytes and PPARγ/thiazolidinedione-induced transactivation in NIH-3T3 fibroblasts. Real-time RT-PCR revealed that thiazolidinedione up-regulates endogenous perilipin mRNA levels. We propose that PPARγ plays a significant role in the transcriptional regulation of murine perilipin gene via the PPRE in its promoter. (*Endocrinology* 145: 2346–2356, 2004)

MAMMALIAN ORGANISMS HAVE the capacity to store energy in adipose tissues. A typical adipocyte contains one or more large cytoplasmic triacylglycerol-rich droplets, surrounded by proteins such as perilipin, adipose differentiation-related protein, and tail-interacting protein of 47 kDa (TIP47) (1). Perilipins, identified by Londos and colleagues (2), are phosphoproteins, the expression of which was restricted to adipocytes and steroidogenic cells (3–5), whereas adipose differentiation-related protein and TIP47 are expressed ubiquitously (1). Murine perilipins consist of four isoforms of perilipin A, B, C, and D, encoded by a single copy gene with alternative and tissue-specific mRNA splicing (6). Perilipin A and B are expressed in both adipocytes and steroidogenic cells, whereas perilipin C and D are detected only in the latter cells. Each isoform of perilipins has a common amino-terminal region and has a unique carboxy-terminal end. The relationship between a molecular profile and tissue distribution of each isoform remains unclear (6). Perilipin A, the most abundant isoform in murine adipose tissue and differentiated cultured 3T3-L1 adipocytes (4), functions to increase triacylglycerol storage by decreasing the rate of triacylglycerol hydrolysis, and thus is fundamental to enlarging lipid droplets in adipocytes (7). Perilipin A has multiple phosphorylation sites within the molecule that are induced by protein kinase A (2). An important step of lipolysis in adipocytes is the translocation of hormone-sensitive lipase (HSL) from cytosol to the surface of the lipid droplet. Recent studies revealed that translocation of HSL required phosphorylation of both HSL and perilipin (8, 9). Conversely, perilipin A provides a protective barrier against lipolysis in the absence of protein kinase A stimulation.

Obesity, an excessive accumulation of adipose tissue, is a major risk factor for hypertension, impaired glucose tolerance, and hyperlipidemia (10). Aggregation of these disorders, referred to as metabolic syndrome, which is otherwise known as insulin resistance syndrome, leads to atherosclerosis and to cardiovascular disease (10). Morphologically, subjects with severe obesity have an increased number (hyperplasia) and size (hypertrophy) of fat cells concomitant with an increase in the size of lipid droplets. Hypertrophic fat cells increase insulin resistance-inducible factors, *e.g.* TNF-α, free fatty acid, and so on (10).

Troglitazone, one of the thiazolidinediones, improves insulin resistance and increases the number of small adipocytes containing small lipid droplets in white adipose tissues of obese Zucker rats, presumably via activating peroxisome proliferator-activated receptor (PPAR) γ (11). Another study demonstrated that adipocytes in heterozygous PPARγ-deficient mice are smaller than those in wild-type mice (12). Thus, the size rather than the number of adipocytes plays an

Abbreviations: C/EBP, CCAAT/enhancer-binding protein; CIP, calf intestinal alkaline phosphatase; DR1, direct repeat 1; FBS, fetal bovine serum; GEMSA, gel EMSA; HSL, hormone-sensitive lipase; mPPAR, murine PPAR; PPARγ, peroxisome proliferator-activated receptor γ; PPRE, PPAR-responsive element; RACE, 5′-rapid amplification of cDNA ends; RLM, RNA ligase-mediated; SV40, simian virus 40; TAP, tobacco acid pyrophosphatase; TSS, transcription start site.

Endocrinology is published monthly by The Endocrine Society (http://www.endo-society.org), the foremost professional society serving the endocrine community.

important role in the pathogenesis of insulin resistance, although it is not well known how PPARγ regulates the size of lipid droplets.

There are reports describing the regulation of perilipin expression. TNF-α decreases perilipin A mRNA by counteracting insulin. On the other hand, BRL 49653, another thiazolidinedione, increases perilipin A mRNA in fully differentiated 3T3-L1 adipocytes (13–15), which suggests that activation of PPARγ may up-regulate perilipin A mRNA in adipocytes, although it is unclear whether signals via PPARγ are directly related to the regulation of perilipin A expression. Because data on the transcriptional regulation of the murine perilipin gene have not been documented, we analyzed the promoter region of this gene and identified a *cis* regulatory element involved in gene expression during differentiation of 3T3-L1 adipocytes.

Materials and Methods

Materials

Dexamethasone and 3-isobutyl-2-methylxanthine were purchased from WAKO Pure Chemicals (Richmond, VA). Insulin and GW9662 were purchased from Sigma Chemical Co. (St. Louis, MO). Pioglitazone was kindly provided by Takeda Chemical Industries (Osaka, Japan). 3T3-L1 preadipocytes and NIH-3T3 fibroblasts were purchased from the American Tissue Culture Collection (Manassas, VA). The anti-PPARγ antibody, PPARγ N-20X, was purchased from Santa Cruz Biotechnology (Santa Cruz, CA).

Isolation of the 5′ untranslated region of the murine perilipin gene

Poly(A)$^+$ RNA was prepared using the Fastrack mRNA isolation kit according to the manufacturer's protocol (Invitrogen Corp., Carlsbad, CA). The 5′-rapid amplification of cDNA ends (RACE) procedure was done using the MARATHON cDNA Amplification kit according to the manufacturer's protocol (Clontech Laboratories Inc., Palo Alto, CA). Two micrograms of poly(A)$^+$ RNA derived from mouse adipose tissues were reverse transcribed and used as a template. Gene-specific antisense primers for 5′-RACE were synthesized based on the sequence obtained from the mouse expressed sequence tag database (dEST). PCR was done using AmpliTaq GOLD DNA polymerase (PerkinElmer Corp., Foster City, CA) and primers (all specific oligonucleotide primers used in these studies are listed in Table 1) mperiAS1 and the adaptor primer (CAP-1) (5′-CCATCCTAATACGACTCACTATAGGGC) provided with the kit. PCR conditions were as follows: denaturing at 94 C for 1 min, annealing at 55 C for 1 min, and extension at 72 C for 3 min; cycle number was 30. The PCR products were gel-purified, subcloned into the TA cloning vector (Invitrogen Corp.), and sequenced using a Big Dye Terminator cycle sequence kit (Applied Biosystems, Foster City, CA).

Isolation of the 5′-flanking region of the murine perilipin gene

Phage clones (1.2×10^6) from 129SV/J mouse genomic library (Stratagene, La Jolla, CA) were screened using a [^{32}P]-labeled 175-bp 5′-RACE product according to standard method (16). After purification and mapping of the positive clones, a 4.3-kb *Xba*I fragment containing the first exon was subcloned into pBluescript II SK-vector (pBS) at an *Xba*I site (designated pX4.3). A 2.9-kb *Xba*I/*Pst*I fragment was subcloned into pBS at an *Xba*I and *Pst*I site (designed pX/P2.9), and both strands were sequenced.

RNA ligase-mediated rapid amplification of cDNA ends

Total RNA was extracted using an RNeasy mini kit according to the manufacturer's protocol (Qiagen, Bothell, WA). To obtain full-length 5′-untranslated region of the perilipin cDNA, RNA ligase-mediated (RLM)-RACE method was used according to the manufacturer's instructions with the FirstChoice RLM-RACE kit (Ambion Inc., Austin, TX), which is designed to amplify cDNA only from full-length, capped mRNA. Briefly, 10 μg of total RNA derived from 3T3-L1 adipocytes 4 d after differentiation was treated with calf intestinal alkaline phosphatase (CIP) for 1 h at 37 C then subjected to phenol/chloroform (1:1, vol/vol) extraction and ethanol precipitation. CIP-treated RNA was incubated with tobacco acid pyrophosphatase (TAP) for 1 h at 37 C to remove the 7-methylguanosine cap at structures from mRNA, leaving the 5′-monophosphates to be ligated to an RNA adaptor with T4 RNA ligase. After reverse transcription with random decamers, PCR was done using primer mperiAS2 and an outer RNA adaptor primer provided with the kit. PCR conditions were as follows: preheat denaturing at 95 C for 9 min, followed by 35 cycles of denaturing at 95 C for 30 sec, annealing at 55 C for 30 sec, and extension at 72 C for 30 sec. Nested PCR was done using primer mperiAS1 and an inner RNA adaptor primer provided with the

TABLE 1. Sequences of oligonucleotides

Name	Use	Nucleotide sequences (5′-3′)	
mperiAS1	mperi: genomic cloning, 5′-RACE, primer extension analysis, RLM-RACE, and RT-PCR	TCACCACAGGCAGCTGCAGAACTC	AS
mperiAS2	mperi: primer extension analysis, RLM-RACE and RT-PCR	GTGCTGTTGTAGGTCTTCTGGAAGC	AS
mperiRT1S	mperi: RT-PCR	TTTGCCCTCCTCTAGCTGGG	S
mperiRT2S	mperi: RT-PCR	GCATTGCCAAGATTCCCTGG	S
mperiLucS1	mperi: pGL3(−2259/+103)	AGGTACCTGACACAGCACACGTCTCAGTG	S
mperiLucS2	mperi: pGL3(−2008/+103)	AGGTACCTTAGGATCTGCCTGGCGCTTTC	S
mperiLucS3	mperi: pGL3(−1827/+103)	AGGTACCAGTCTCCCAGATTACTCGTCCTG	S
mperiLucS4	mperi: pGL3(−1678/+103)	AGGTACCTGGAAGCTCCTTGTTCCACACC	S
mperiLucS5	mperi: pGL3(−1442/+103)	AGGTACCACACCCGCACTTATACACATGCTC	S
GLprimer2	mperi: pGL3s	CTTTTATGTTTTTGGCGTCTCCA	AS
mperipLucS1	mperi: pGL3-pr(−2008/−1802)	AGAGCTCTTAGGATCTGCCTGGCGCTTTC	S
mperipLucS2	mperi: pGL3-pr(−1957/−1802)	AGAGCTCGAATCCGTACAGAAGCAGCCAAA	S
mperipLucS3	mperi: pGL3-pr(−1933/−1802)	AGAGCTCGGCTTTGTCAGCAGAGCT	S
mperipLucS4	mperi: pGL3-pr(−1858/−1802)	AGAGCTCGGCTGCCCTTTAGCCTGGGCTGT	S
mperipLucAS	mperi: pGL3-pros	TGAGCTCCAGGACGAGTAATCTGGGAGAC	AS
mpericodeS	mperi: real-time RT-PCR	AGAGTTCTGCAGCTGCCTGTG	S
mpericodeAS	mperi: real-time RT-PCR	CAGAGGTGCTTGCAATGGGCA	AS
mβactinS	mβactin: real-time RT-PCR	ATATCGCTGCGCTGGTCGTC	S
mβactinAS	mβactin: real-time RT-PCR	AGCACAGCCTGGATGGCTAC	AS
mPPARγS	mPPARγ: RT-PCR	TTGACAGGAAAGACAACGGA	S
mPPARγAS	mPPARγ: RT-PCR	GAGCAGAGTCACTTGGTCATT	AS

Underlines show restriction enzyme sites of *Kpn*I or *Sac*I. S, Sense primer; AS, antisense primer.

kit. PCR conditions were the same as described above. PCR products were directly subcloned using a TOPO TA cloning kit (Invitrogen Corp.). The nucleotide sequences of PCR products were determined by sequencing.

Confirmation of transcription start site (TSS) by RT-PCR

To confirm the TSS, RT-PCR was done using gene-specific sense primers; mperiRT1S and mperiRT2S, upstream and downstream of TSS determined using the RLM-RACE method. The antisense primer used was mperiAS1, located on exon 3. Total RNA (0.5 μg) of 3T3-L1 adipocytes 4 d after differentiation was used in the RT-PCR. RT was done according to the manufacturer's protocol (Superscript III RNase H⁻ Reverse Transcriptase, Invitrogen). PCR conditions were as follows: preheat denaturing at 95 C for 9 min, denaturing at 95 C for 30 sec, annealing at 58 C for 30 sec, and extension at 72 C for 30 sec; cycle number was 30. PCR products were analyzed electrophoretically using 2.5% agarose gels.

Plasmid construction

After the digestion of pX/P2.9 with *Eco*RV and *Pst*I, a 2.5-kb DNA fragment was subcloned into *Eco*RV/*Pst*I-digested pBS (designated pE/P 2.5), which was digested with *Kpn*I and *Sma*I, and the DNA fragment was subcloned into *Kpn*I/*Sma*I-digested luciferase expression vector, pGL3 basic vector (Promega, Madison, WI), designated pGL3(−2422/+103). pGL3(−932/+103), pGL3(−504/+103), and pGL3(+64/+103) were generated by digestion with *Hin*cII, *Sac*I, or *Pvu*II as well as *Kpn*I, blunting and self-ligating. pGL3(−219/+103), pGL3(−2008/+103), pGL3(−1827/+103), pGL3(−1678/+103), and pGL3(−1442/+103) were generated by PCR using pGL3(−2422/+103) as template and the specific primers shown in Table 1. PCR products were digested with *Kpn*I and *Pst*I and subcloned into the *Kpn*I/*Pst*I-digested pGL3 basic vector. To further delineate enhancer region, various DNA fragments (−2008 to −1802 bp) were similarly ligated into the minimal simian virus 40 (SV40) containing the pGL3 promoter luciferase expression vector (Promega). The largest promoter construct, designated pGL3pro(−2008/−1802), and subsequent truncated fragments (−1957/−1802, −1933/−1802, and −1858/−1802 bp) were PCR-amplified using pGL3(−2422/+103) as template. These promoter fragments were subcloned into the *Sac*I-digested pGL3 promoter vector. In addition to these forward direction constructs, we generated another series of luciferase constructs in which reverse directional DNA fragments were ligated. The largest promoter construct was named pGL3pro(−1802/−2008), and subsequent truncated constructs were designated as well. Sequences of all primers used are given in Table 1. Purification of plasmids was done using a modified alkaline lysis method (Plasmid Maxi kit, Qiagen), and the vector-insert junctions were confirmed by sequencing.

Mutational modifications of the murine perilipin gene

Mutations of a putative PPAR-responsive element (PPRE) were generated using a QuikChange XL Site-Directed Mutagenesis kit (Stratagene) according to the manufacturer's instructions. Briefly, 10 ng of pGL3pro(−2008/−1802) was used as a template and the mutated nucleotides as described (see Fig. 4B). PCR conditions were as follows: denaturing at 95 C for 1 min, followed by 18 cycles of denaturing at 95 C for 50 sec, annealing at 60 C for 50 sec, and extension at 68 C for 12 min. After digestion with *Dpn*I, 2 μl of PCR products were used to transform XL10-Gold competent cells provided with the kit. Appropriate clones were verified by sequencing.

Cell culture and transfection

3T3-L1 preadipocytes were grown in DMEM containing 10% fetal bovine serum (FBS) and seeded on 12-well plates. Forty-eight hours after reaching confluence, cells began to differentiate under the treatment with 174 nM insulin, 0.5 mM 3-isobutyl-1-methylxanthine, 1 μM dexamethasone, and 1 μM pioglitazone in DMEM containing 10% FBS. After 48 h of incubation, medium was replaced with DMEM only containing 10% FBS, and transfection was done using a LipofectAMINE2000 reagent (Invitrogen Corp.) according to the manufacturer's protocol. Briefly, 2 μl of LipofectAMINE2000 reagent was gently mixed into 100 μl of OPTI-MEM (Life Technologies, Inc./BRL, Rockville, MD) and the preparation incubated for 5 min at room temperature. One microgram of luciferase reporter construct and 0.3 μg of pCMV-SPORT β-gal expression vector (Invitrogen) in 100 μl OPTI-MEM were mixed with 100 μl of reagent containing OPTI-MEM and the mixture incubated for an additional 15 min. After the incubation, transfection mixtures were added to the cells, the preparation was incubated for 48 h, then the cells harvested.

In other experiments, 3T3-L1 preadipocytes and NIH-3T3 fibroblasts were grown to 70–80% confluence in DMEM and 10% FBS, and luciferase reporter constructs were transfected using LipofectAMINE2000 as described above. In NIH-3T3 fibroblasts, a total of 2 μg of various amounts of mPPARγ2 expression vector and mock vector [pSV-CMV vector (17)] was transfected, with or without pioglitazone, in addition to 1 μg of luciferase reporter plasmid. Murine (m) PPARγ2 expression vector was constructed by inserting a PCR-amplified mPPARγ2 cDNA fragment into pSV-SPORT vector (Life Technologies/BRL). The dose of pioglitazone used was 1 μM. Cells were harvested 48 h after transfection. Cells were washed twice with PBS, lysed, and luciferase activities were measured using a TD20/20 luminometer (Turner BioSystems Inc., Sunnyvale, CA) and a Luciferase assay system (Promega). Transfection efficiency was adjusted depending on β-galactosidase activities. Data are presented as fold-increase of luciferase activity over control vector (pGL3 basic or pGL3 promoter vector).

Gel EMSA (GEMSA)

Nuclear extracts were prepared from 3T3-L1 adipocytes 4 d after differentiation using a commercially available kit (NE-PER nuclear and cytoplasmic extraction reagent, PIERCE Chemical Corp., Rockford, IL). GEMSA was done using reagents in the Gel Shift Assay kit (Promega). To analyze the binding of nuclear hormone receptors to the putative PPRE, sense oligonucleotides of probes given in Fig. 6A were end-labeled using [γ^{32}P]ATP (3000 Ci/mmol, 10 mCi/ml Amersham Biosciences, Piscataway, NJ) and T4 polynucleotide kinase using a standard method (16) and were column-purified (Microspin G-25 Columns, Amersham Biosciences) (see Fig. 6A). After annealing with sequence-matched complementary oligonucleotides, these probes were used for GEMSA. The binding reaction was done according to the manufacturer's instructions using 5 μg of nuclear extract and 0.2 pmol of each labeled probe. Competition analysis was made using a 100-fold amount of unlabeled double-stranded oligonucleotides corresponding to the labeled probe. Samples were electrophoresed on 4% polyacrylamide gels in 0.5× TBE buffer (9 mM Tris/HCl, 90 mM boric acid, and 20 mM EDTA, pH 8.0) at 4 C, dried, and analyzed by autoradiography.

Effects of PPARγ agonist and antagonist

The regulation of perilipin mRNA levels by PPARγ agonist and antagonist were examined in differentiated 3T3-L1 adipocytes. 3T3-L1 preadipocytes were cultured and differentiated as described above. Pioglitazone, a PPARγ agonist, was added to the media 48 h after differentiation. On the other hand, GW9662, a PPARγ antagonist, was added to the media at the beginning of differentiation. Both reagents were maintained until the cells were harvested.

Expression analysis of perilipin mRNA by real-time RT-PCR

Two micrograms of total RNA of 3T3-L1 adipocytes 4 d after differentiation-treated with PPARγ agonist and antagonist were reverse transcribed in a 20-μl reaction volume. Real-time PCR was performed using ABI PRISM 7700 Sequence Detection System and SYBR Green I as a double-stranded DNA-specific binding dye, according to the manufacturer's instructions (PE Applied Biosystems, Foster City, CA). Amplifications were carried out using 15 μl SYBR Green PCR mastermix (Applied Biosystems), 11.2 μl sterile deionized water, 2 μl reverse transcript sample, and 1.8 μl primer pair (30 nM) in a 30-μl reaction volume. The real-time PCR conditions were as follows: preheat denaturing at 95 C for 10 min, followed by 40 cycles of heat denaturing at 95 C for 30 sec, annealing at 55 C for 30 sec, and extension at 72 C for 1 min. The melting temperature profile for perilipin and β-actin demonstrated single peak

at 87 and 88 C, respectively. The interassay and intraassay coefficients of variation were calculated to be 5.9 and 2.2%, respectively, using primers for β-actin and reverse transcript sample.

Primer sequences used are described in Table 1. Primers were designed to recognize a different exon in each gene, and the size of PCR products was verified by agarose gel electrophoresis. Exogenous cDNA standards for perilipin and β-actin were produced by inserting PCR products, which were generated using sample primers noted above and 3T3-L1 adipocytes cDNA as templates, into the pCR2.1 vector using the TOPO TA cloning kit. Inserts of control vectors for perilipin and β-actin were verified by sequencing. The concentration of each standard was determined by measuring the OD260, and the copy number was calculated. The β-actin was quantified to normalize perilipin mRNA levels, and the final results were expressed as the ratio of the copy number of perilipin to the copy number of β-actin.

Expression of PPARγ mRNA of each sample was validated by RT-PCR using specific primers. PCR conditions were as follows: preheat denaturing at 95 C for 9 min, denaturing at 95 C for 30 sec, annealing at 55 C for 30 sec, and extension at 72 C for 30 sec; cycle number was 30. PCR products were analyzed electrophoretically using 2.5% agarose gels.

DNA sequence analysis

We used the web-based search programs Transcription Element Search Software (TESS) (http://www.cbil.upenn.edu/tess/) and TRANSFAC (http://transfac.gbf.de/TRANSFAC/) to analyze the 5′-flanking region of the perilipin gene. In addition to these programs, we visually inspected minimal suspicious promoter regions.

Results

Determination of TSS

Because the nucleotide sequence of perilipin cDNA had not been reported when our experiment was started, we searched an expressed sequence tag database (dEST) using a 200-bp sequence of the rat and human perilipin cDNA located around the translation initiation site. Two antisense primers (mperiAS1 and mperiAS2) were generated based on the sequence hit (GenBank accession nos. AA458173, AA510052, AA711707, AA982036, AI158797, and AI180560). Primer extension analysis, 5′-RACE, and RLM-RACE were done using these antisense primers.

Initially, the standard 5′-RACE and primer extension analysis were done to determine TSS (data not shown). While doing these experiments, the nucleotide sequence of mouse perilipin cDNA was reported (6). Because TSS derived from our experiments was incompatible with that described in the report, RLM-RACE was done. With this method, cDNA is generated only from full-length, capped mRNA, by treatment of RNA with CIP and TAP before reverse transcription. The PCR products obtained by RLM-RACE showed a broad band from approximately 120–210 bp (lane 1 in Fig. 1A). Sequencing of the PCR products showed that they were

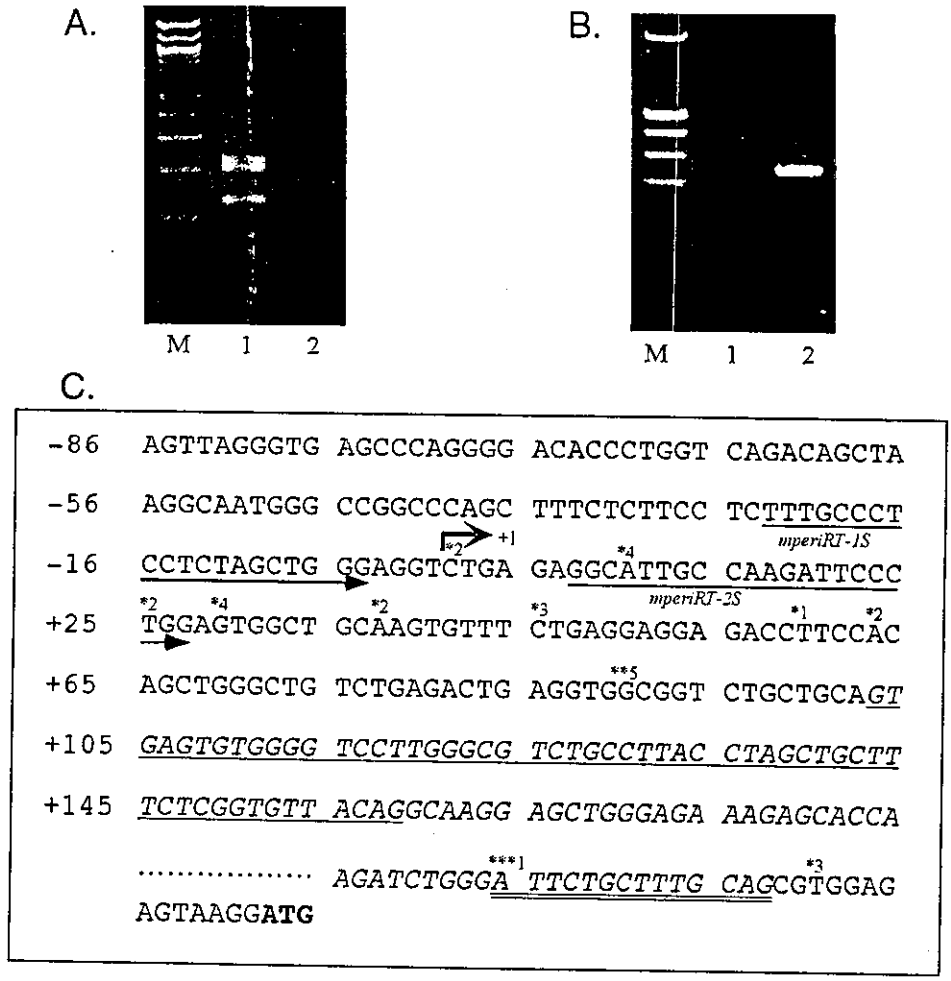

FIG. 1. Determination of the TSS of murine perilipin gene. A, Gel electrophoresis of the PCR product, deduced from RLM-RACE experiments with (lane 1) and without TAP treatment (lane 2); 100-bp DNA ladder (lane M). B, Gel electrophoresis of PCR product, obtained using RT-PCR and a gene-specific sense primer located upstream (mperiRT1S, lane 1) and downstream (mperiRT2S, lane 2) of TSS determined by RLM-RACE. The antisense primer was located in exon 3 (mperiAS2); 100-bp DNA ladder (lane M). C, Genomic DNA sequence in the vicinity of TSS of mouse perilipin gene. *Bold, right-angled arrow* and +1 indicate the most upstream TSS deduced from RLM-RACE experiment. Sense primers used in RT-PCR experiment are indicated by *arrows*. Figure with *asterisks* indicated *above the sequence* shows number of the clones in which the 5′ end of cDNA was determined by sequencing (a total of 29 clones were sequenced). The clone with a *single asterisk* indicated *above the sequence* lacks a DNA segment shown by a *single underline*. However, the clone with *double asterisks* has a *single underline* sequence. The clone with *triple asterisks* has another alternative splicing; additional DNA segment indicated by *double underlines*. The sequence shown by italic letters corresponds to the intron of major mRNA. *Bold letters* indicate a translation initiation codon, ATG.

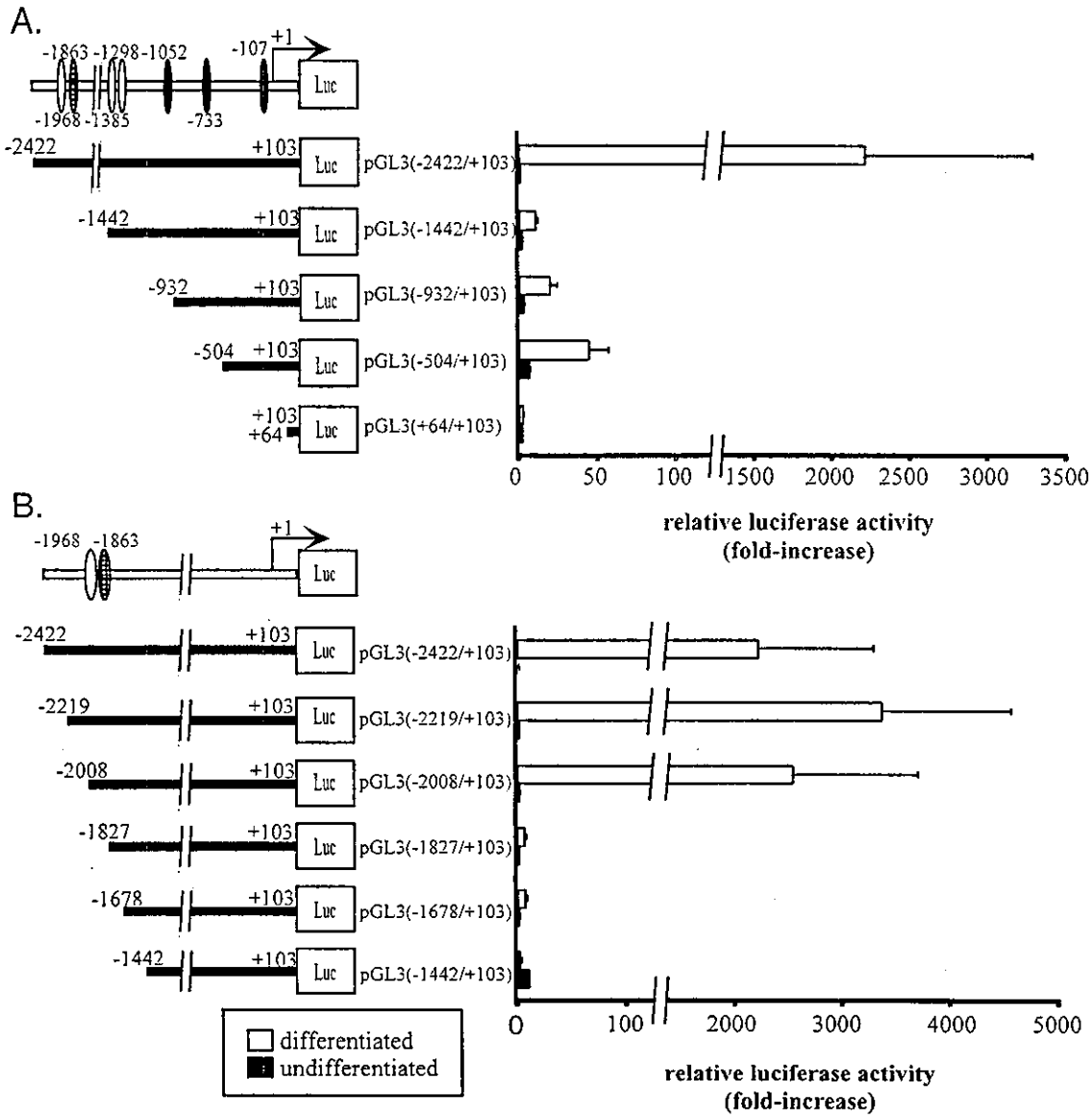

FIG. 2. Luciferase activities of the murine perilipin promoter in 3T3-L1 cells. A, Luciferase assay using fused promoter constructs. B, Luciferase assay using constructs abbreviated at approximately 200-bp length from −2242 to −1442 bp. The locations of putative *cis* regulatory elements are indicated by *open* (PPRE), *closed* (C/EBPα), and *checkered* (C/EBPβ) *vertical ovals on the top solid line* and directionally localized by the first base pair of each motif. At least three experiments were carried out in duplicate. Normalized luciferase activities are shown as the means ± SEM. Luc, Luciferase.

composed of several kinds of clones (11 different clones of the 29 sequenced) (Fig. 1C). Three alternative splicings were evident with a little difference compared with the previous report (6) (Fig. 1C). Presumably, the RLM-RACE experiment revealed that the 5′ end of the longest cDNA was extended 7 bp upstream compared with that in previous report (6) and was designated +1 as TSS (Fig. 1C; *bold right-angled arrow*). Analysis of sequences in the promoter region revealed no canonical TATA, CAAT, or GC motif in the murine perilipin gene, as there was no typical initiator sequence.

To confirm the TSS, a RT-PCR experiment was done using a gene-specific sense primer upstream and downstream of the TSS determined by RLM-RACE (mperiRT1S and mperiRT2S, respectively, in Fig. 1C). When the upstream sense primer was used, no PCR product could be detected (lane 1 in Fig. 1B). Two bands yielded by alternative splicing were found when the downstream sense primer was used (lane 2 in Fig. 1B). These results indicate that mRNA encoding mouse perilipin protein did not extend to the position of upstream sense primer.

Identification of cis regulatory element(s) in the 5′-flanking region of the perilipin gene

To identify upstream *cis* element(s), a series of 5′ deletion reporter constructs were generated and transfected into

3T3-L1 cells before and 2 d after differentiation to measure luciferase activity. No significant change of luciferase activity was detected when 3T3-L1 preadipocytes were used (Fig. 2A). However, when transfected into differentiated 3T3-L1 adipocytes, the constructs showed a significant reporter gene activity. Especially, the construct with the largest DNA fragment [pGL3(−2422/+103)] revealed approximately 2000-fold luciferase activity compared with that of pGL3 basic vector (Fig. 2A). When the 5′ end of DNA fragment was shortened to −1442 bp, luciferase activity prominently diminished. Then, to further analyze the region between −2422 and −1442 bp, additional reporter gene constructs [pGL3(−2219/+103), pGL3(−2008/+103), pGL3(−1827/+103), and pGL3(−1678/+103)] were generated, and luciferase activity was measured (Fig. 2B). When the 5′ end of reporter gene constructs was abbreviated from −2008 to −1827 bp, the reporter activity was prominently diminished.

To further delineate location of the *cis* element(s), another series of 5′ truncated constructs were generated. Sequential DNA segments ranging from −2008/−1802 to −1858/−1802 bp were ligated to the upstream of the minimal SV40 promoter in pGL3-promoter vector (Fig. 3A). The longest construct, containing the −2008 to −1802-bp DNA segment, consistently showed more than a 10-fold higher luciferase activity than did the insertless pGL3 promoter vector when transfected into differentiated 3T3-L1 adipocytes. In contrast, no different luciferase activity could be detected in 3T3-L1 preadipocytes. The experiments with reverse direction vec-

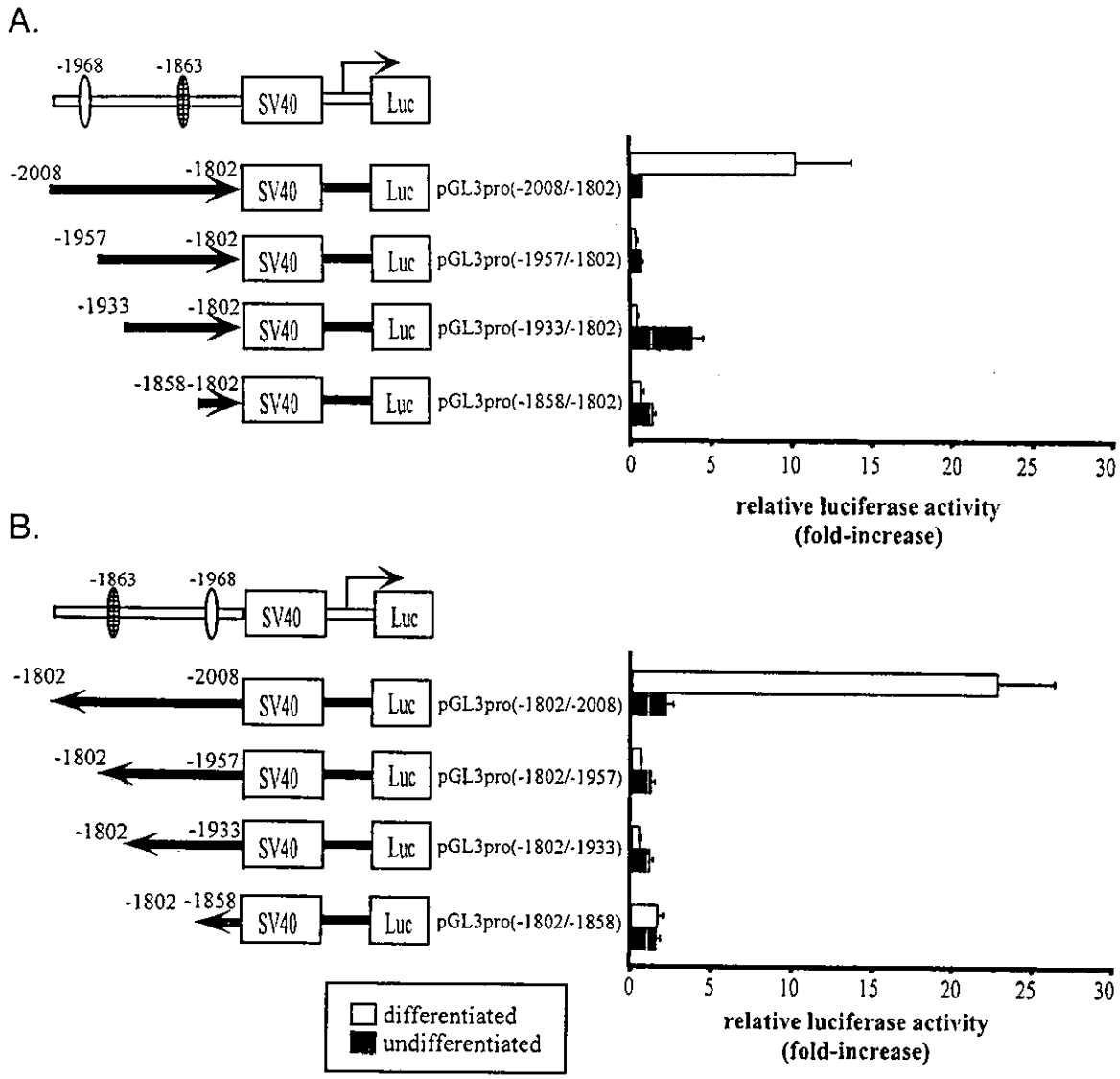

FIG. 3. Luciferase activities of murine perilipin promoter ligated pGL3-promoter vector in 3T3-L1 cells. A, Sequential DNA segments ranging from −2008/−802 bp to −1858/−1802 bp were ligated to upstream of the minimal SV40 promoter in pGL3-promoter vector as described in *Materials and Methods*. B, DNA fragments ligated reverse directionally in panel A to upstream of the minimal SV40 promoter in pGL3-promoter vector. The locations of putative *cis* regulatory elements are indicated by *open* (PPRE) and *checkered* (C/EBPβ) *vertical ovals on the top solid line*. At least three experiments were done in duplicate. Normalized luciferase activities are shown as the means ± SEM. Luc, Luciferase.

tors gave the same results (Fig. 3B). Taking these data together, a 51-bp region located within −2008 bp to −1957 bp seems to be critical to up-regulate the perilipin gene transcription during adipocyte differentiation.

Identification of a functional PPRE in the 5′-flanking region of the mouse perilipin gene

In comparison with functional PPRE identified in other genes, a minimal 51-bp region between −2008 bp to −1957 bp seemed to contain a putative PPRE at −1980 bp to −1968 bp (Fig. 4B), which is similar to direct repeat 1 (DR1) motifs (Fig. 4A). The pGL3pro(−2008/−1802) vector was then transfected into NIH-3T3 fibroblasts with 0–2 μg of the mPPARγ2 expression vector (Fig. 4C). In this experiment, PPARγ2 with PPARγ ligand, pioglitazone, augmented reporter gene activity in a dose-dependent manner, whereas PPARγ2 alone weakly increased the reporter activity. These results indicated that PPARγ2 functioned via this PPRE, either directly or indirectly.

GEMSA

Nuclear extracts from differentiated 3T3-L1 adipocytes were incubated with radiolabeled wild-type (PPRE wild-type) and two mutant PPRE probes with different positions (PPREmut and PPRE3mut) plus or minus unlabeled competitors (Fig. 5A). When the radiolabeled wild-type probe was used, an up-shifted band was detected (lane 1 in Fig. 5B). The signal of the shifted bands disappeared by competition with an excessive amount of the unlabeled wild-type probe (lane 2 in Fig. 5B), but not with the mutant-type probes (lanes 4 and 5 in Fig. 5B). The radiolabeled wild-type probe with antibody against PPARγ produced a supershifted band (lane 3 in Fig. 5B). When radiolabeled mutant type probes were used, no shifted bands were produced (lanes 6 and 7 in Fig. 5B).

Mutational analysis of putative PPRE

To determine whether putative PPRE was functional as the element bound to PPARγ, transfection experiments were

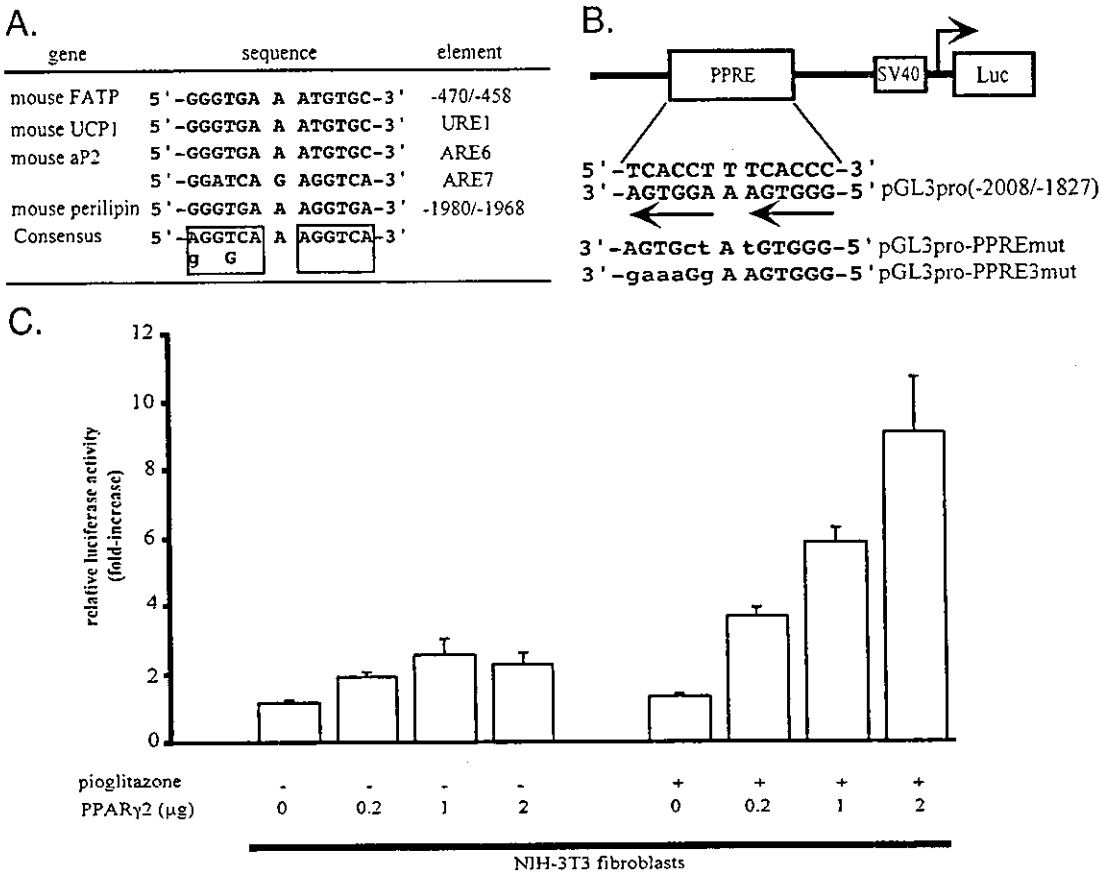

FIG. 4. Identification of PPRE in the 5′-flanking region of the mouse perilipin gene. A, PPRE in the 5′-flanking region of the mouse perilipin gene is compared with the PPRE sequence in various murine PPARγ-responsive genes: mouse FATP (fatty acid transport protein) PPRE (18); mouse UCP1 (uncoupling protein 1) PPRE (31); aP2 (adipocyte fatty acid binding protein 2) PPRE, *ARE6* and *ARE7* (19); and consensus PPRE sequence (18). DR1 motif is *boxed*. B, A scheme of luciferase constructs using transfection experiments. The sequences of PPRE wild-type, pGL3pro(−2008/−1802), and two kinds of mutated constructs (mut), pGL3pro-PPREmut and pGL3pro-PPRE3mut, are described. *Small letters* indicate mutated nucleotides. C, pGL3pro(−2008/−1802) vectors were transfected into NIH-3T3 fibroblasts with a total 2 μg of mPPARγ2 expression vector and pSV-CMV mock vector with or without 1 μM pioglitazone. At least three experiments were done in duplicate. Normalized luciferase activities are shown as the means ± SEM.

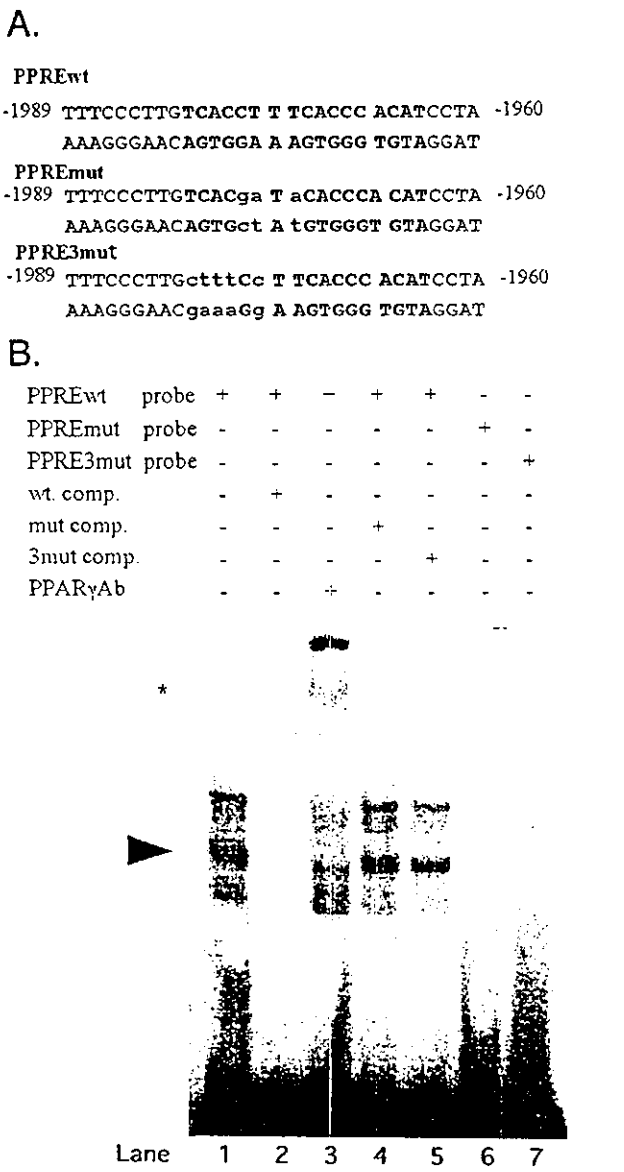

FIG. 5. GEMSA using nuclear extracts of differentiated 3T3-L1 adipocytes. A, Nucleotide sequences of wild-type (PPREwt) and two mutant PRE probes with different positions (PPREmut and PPRE3mut); PPRE is shown by *bold lettering*, and *small letters* indicate mutated nucleotides. B, Result of GEMSA. Ratio of competitor (comp.) to labeled probe was 100:1. *Arrowhead* indicates a probe-nuclear extract complex. A supershifted band with PPARγ antibody is indicated by an *asterisk*.

done using two kinds of mutated pGL3pro(−2008/−1802) vector and two cell lines, NIH-3T3 fibroblasts and 3T3-L1 adipocytes (Fig. 6). In the experiment using NIH-3T3 fibroblasts, luciferase activities were diminished in the presence of PPARγ2 and pioglitazone when each mutated pGL3pro(−2008/−1802) vector was transfected (Fig. 6A). In addition, luciferase activities of both mutated constructs were significantly reduced compared with that of wild-type pGL3pro(−2008/−1802) in experiments using differentiated 3T3-L1 adipocytes (*right columns* in Fig. 6B). These results indicated that the ability to respond to PPARγ lies within the DR1-type PPRE.

Regulation of perilipin mRNA levels by PPARγ agonist and antagonist in differentiated 3T3-L1 adipocytes

Finally, we examined whether endogenous perilipin gene was regulated by PPARγ. For this purpose, real-time RT-PCR was used to quantify perilipin mRNA levels in differentiated 3T3-L1 adipocytes treated with different concentrations of PPARγ agonist and antagonist. As shown in Fig. 7A, increasing concentrations of pioglitazone resulted in a dose-dependent increase in perilipin mRNA. On the other hand, GW9662 was able to decrease perilipin mRNA and reduce the effect of pioglitazone in a dose-dependent manner. Meanwhile, PPARγ mRNA of each condition was expressed in a similar manner. The effect of PPARγ agonist and antagonist for perilipin gene was also revealed in the reporter activity of pGL3(−2422/+103), containing the full murine perilipin promoter, transfected into differentiated 3T3-L1 adipocytes (Fig. 7B). These findings indicated that identified PPRE functions to regulate transcriptional levels on the murine perilipin gene in differentiated 3T3-L1 adipocytes.

Discussion

The first purpose of the current study was to confirm the TSS of murine perilipin mRNA. Our data of TSS determined by primer extension analysis and a standard 5′-RACE procedure (data not shown) did not correspond to findings in a previous report (6). The RLM-RACE procedure was done and resulted in identification of the existence of multiple transcription start sites. The promoter region in the murine perilipin gene has no canonical TATA, CAAT, and GC motif. In addition, there are no typical initiator sequences around TSS. These appear to be responsible for the diversity of start sites.

The second purpose was to identify regulatory factor(s) during adipocyte differentiation by analyzing the 5′-flanking region of perilipin gene. Consequently, a functional PPRE was identified and proved to be a key element in transcriptional activation of the murine perilipin gene during adipogenesis. Perilipin, one of the genes related to lipid metabolism as are CD36, adipocyte fatty acid binding protein, fatty acid transport protein, and acyl-coenzyme A synthetase, which also have functional PPRE in the promoter region (18–21), is a possible candidate gene regulated by this group of nuclear transcription factor, PPARs. Previous studies have shown that treatment of fully differentiated 3T3-L1 adipocytes with thiazolidinediones, which activate PPARγ, leads to an increase in murine perilipin mRNA or protein (13–15). A sequence in the 5′-flanking region of the murine perilipin gene identified in our study is similar to the consensus sequence of previously identified PPREs (see Fig. 4A).

Real-time RT-PCR experiments revealed that transcription of perilipin mRNA can be activated in a dose-dependent fashion by pioglitazone and inhibited in a dose-dependent fashion by GW9662. Additionally, transfection experiments using pGL3(−2422/+103) into differentiated 3T3-L1 adipocytes showed that full murine perilipin promoter containing identified PPRE is regulated by pioglitazone and GW9662.

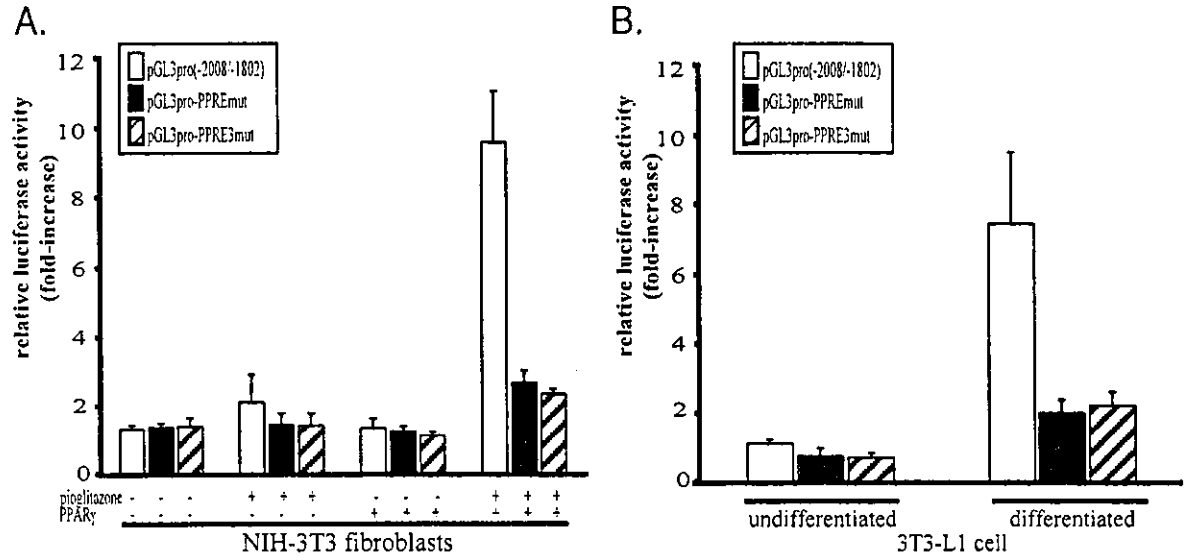

FIG. 6. Mutational analysis of putative PPRE. A, pGL3pro(−2008/−1802) vector and two kinds of mutated pGL3pro(−2008/−1802) vectors were transfected into NIH-3T3 fibroblasts under different conditions of mPPARγ2 expression vector and pioglitazone. B, pGL3pro(−2008/−1802) vector and two kinds of mutated pGL3pro(−2008/−1802) were transfected into 3T3-L1 cells under undifferentiated and differentiated conditions. At least three experiments were done in duplicate. Normalized luciferase activities are shown as the means ± SEM.

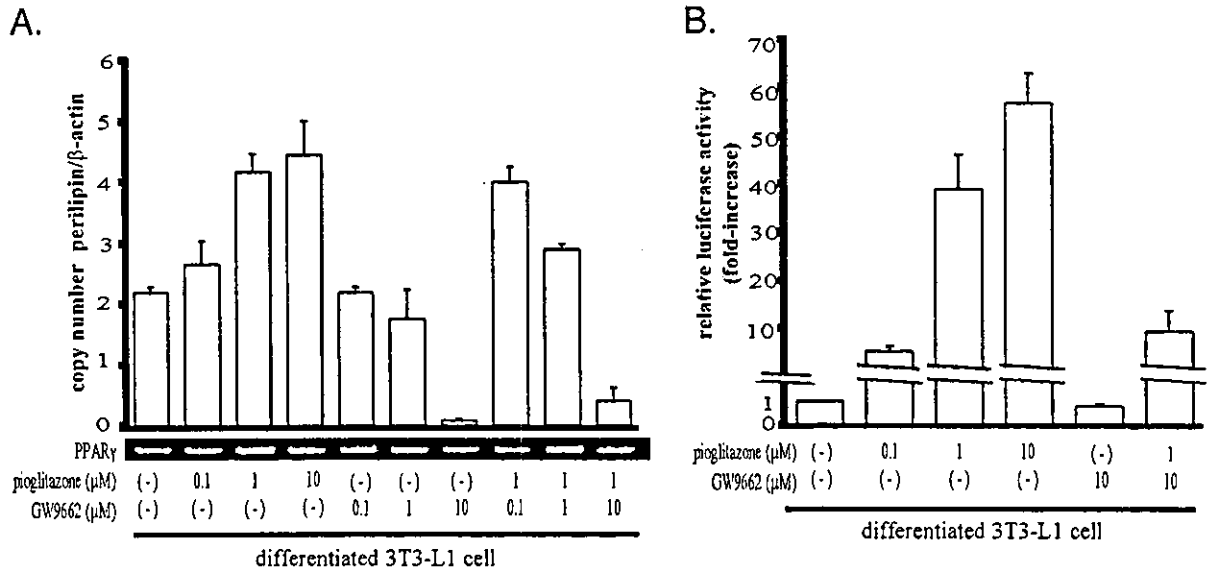

FIG. 7. Regulation of endogenous perilipin mRNA by PPARγ agonist and antagonist in differentiated 3T3-L1 adipocytes. A, Expression of murine perilipin mRNA in differentiated 3T3-L1 adipocytes under different conditions of pioglitazone and GW9662, as determined by real-time RT-PCR. *Column heights* represent the mean ratio of the mRNA copy number of perilipin to the mRNA copy number of β-actin. At least three experiments were done in duplicate. *Error bar* indicates SEM. Expression of mPPARγ mRNA detected by RT-PCR was shown. B, pGL3(−2422/+103) containing the full murine perilipin promoter transfected into differentiated 3T3-L1 adipocytes treated with pioglitazone and GW9662. At least three experiments were done in duplicate. Data are calculated as fold-increase of luciferase activity over control condition [pioglitazone (−) and GW9662 (−)] and are shown as the means ± SEM.

These results demonstrated that endogenous perilipin mRNA levels are regulated by PPARγ and its ligands via identified PPRE. These findings support the notion that the expression of murine perilipin mRNA is limited in tissues expressing PPARγ mRNA (19, 22).

PPARγ is a key transcriptional nuclear factor that regulates not only adipogenesis but also glucose and lipid metabolism. Previous studies using PPARγ null embryonic fibroblasts (12) revealed that PPARγ is essential for adipogenesis. Furthermore, CCAAT/enhancer-binding protein (C/EBP) α, adipocyte determination- and differentiation-dependent factor 1/sterol regulatory element binding protein 1c, and other transcriptional factors expressed in adipocytes, are regulated downstream of PPARγ. Our present study revealed that perilipin is another gene regulated downstream of PPARγ during adipogenesis. Kubota *et al.* (12) demonstrated that the

```
mPeri -2014 CTTAGGA-TCTGCCTGGCGCTTT---CCCTTGTCACCTTTCACCCACATCCTAGAATCCG -1955
hPeri -3309 CTCGGGACTCTCCTAGGCCCTTTCACCACTTCTCACCTCTCACCCACATTCTGCACTCCC -3250

mPeri -1954 TACAGAAGCAGCCAAAGGACCGGCTTTGTCAGCAGAGCTTTCAGGCACAGAGCCCTATAT -1895
hPeri -3249 AGCTAAAGCAGCCAAAGGACTATTTGATTTGGCAGAGCTTTCAGGCACAAAGCCCTATGT -3190

mPeri -1894 CCTCTCTGGCCCAAAGCCACTGCCTGGGAAGGC---AGGCTGCCCTTTAGCCTGGGCTG- -1835
hPeri -3189 TCCCTCTGGCCCAAAGCCACT-ACTCTGAAGGCTGAAAACTGCCCTTTGGCTCAGGTTGC -3130

mPeri -1834 TGTCCAGATGCAAGTCTCCCAGATTACTCGTCCTG..... -1800
hPeri -3129 TGTCCAG-TCACAGCCTCACAGATAATTTGTGCTG..... -3096
```

FIG. 8. Alignment of the nucleotide sequences in the vicinity of PPRE in the murine perilipin (mPeri) gene and its human counterpart (hPeri). In human perilipin gene, sequence number is designated adenosine of translation initiation codon, ATG, as +1. PPRE of murine perilipin gene and PPRE like sequence of its human gene are *boxed*. Identities are indicated by *screen background*. There is a 71.8% homology within this region.

size of adipocytes is smaller in heterozygous PPARγ-deficient mice [PPARγ$^{(+/-)}$] than in the wild-type under conditions of a high-fat diet. Taking our results into account, morphological change of adipocytes in PPARγ$^{(+/-)}$ mice may be due to suppression of perilipin expression by loss of one PPARγ allele.

Overexpression of perilipin in 3T3-L1 preadipocytes led to an accumulation of numerous small lipid droplets (7), and mutant perilipin transfections into NIH-3T3 fibroblasts or Chinese hamster ovary cells resulted in inhibitory effects on hormone-mediated lipolysis (8, 9). A recent study demonstrated that adipocytes in perilipin-null mice [*Peri*$^{(-/-)}$] were smaller than in wild-type mice and prevented body weight gain under conditions of a high-fat diet (23). Serum leptin, which is one of insulin-sensitizing adipocytokines, is increased in *Peri*$^{(-/-)}$, whereas PPARγ mRNA expression in adipocytes is unchanged (23). Another study on perilipin knockout mice showed that breeding the *Peri*$^{(-/-)}$ alleles into *Lpr*$^{db/db}$ mice reversed the obesity (24). These results suggest that perilipin may participate in signaling mechanisms related to energy homeostasis, independent of PPARγ activation.

Assessing a role of PPARγ in the pathogenesis of obesity is difficult. It was reported that PPARγ antagonist reduced body weight and insulin resistance in *KKAy* mice on high-fat diet (25). This indicates that PPARγ antagonist has potential as an antiobesity drug. However, a more recent study revealed that PPARγ may induce synthesis of adiponectin, known as the antidiabetic (26) and antiatherogenic (27) adipocytokine. Therefore, control of PPARγ expression may aggravate metabolic conditions. Although direct suppression of perilipin gene expression may be a therapeutic target for obesity, further supportive study is needed. Otherwise, enhanced energy expenditure, which is accompanied by lipolysis in adipocytes, is another strategy of therapy for obesity. It is reasonably postulated that constitutional activating phosphorylation of perilipin may prevent maturing of lipid droplets. Recently, Wang *et al.* (28) showed that PPARδ, which binds PPRE, inhibited obesity by activating fat burning. It was not mentioned whether PPARδ affects expression of perilipin. Our GEMSA experiments demonstrated two extra bands in addition to a main shifted band. These extra bands remain, even when using specific PPARγ antibody, indicating that identified PPRE may bind to other ligands such as PPARδ. PPARδ may repress PPARγ-mediated transcriptional activity (29). Thus, it will be of interest to determine whether expression of the perilipin gene is controlled by PPARδ through the identified PPRE. Furthermore, it was not clarified whether increase of phosphorylated perilipin modulates energy expenditure. The relationship between PPARδ activation and phosphorylated perilipin in fat burning requires attention.

Finally, Nishiu *et al.* (30) isolated human perilipin cDNA and identified the gene on human chromosome 15. At this time, the human perilipin promoter has not been analyzed. We compared the sequences between human chromosome 15 upstream of the perilipin gene (GenBank accession nos. AC079075 and NM_002666) and the 5′-flanking region of the murine perilipin gene and identified the PPRE-like sequence at −3277 to −3265 in the human genome (adenosine of translation initiation codon, ATG, is designated +1), which is the DR1 type of PPRE and is similar to the PPRE of the murine perilipin gene identified in the present study. Whereas there is a 65% homology within a 500-bp region upstream of TSS between the murine and human perilipin gene, the nucleotide identity within a region of more than 500 bp upstream of TSS was generally less than 50%. However, nucleotide sequences in the vicinity of this PPRE-like motif are highly conserved between human and murine perilipin gene (71.8% in 201 bp) (Fig. 8). It will be of interest to determine whether these elements in human perilipin function as well.

Acknowledgments

We thank M. Ohara (Fukuoka, Japan) for critical reading of the manuscript and M. Ishida (Hokkaido University) for expert technical assistance.

Received September 8, 2003. Accepted January 8, 2004.

Address all correspondence and requests for reprints to: Chikara Shimizu, M.D., Ph.D, Department of Medicine II, Hokkaido University Graduate School of Medicine, N-15, W-7, Kita-ku, Sapporo 060-8638, Japan. E-mail: shimizch@med.hokudai.ac.jp.

This work was supported in part by a Grant-in-Aid for Scientific Research (C: 15590965) from the Ministry of Education, Culture, Sports, Science and Technology, Japan (to C.S.).

References

1. Miura S, Gan, JW, Brzostowski J, Parisi MJ, Schultz CJ, Londos C, Oliver B, Kimmel AR 2002 Functional conservation for lipid storage droplet association among Perilipin, ADRP, and TIP47 (PAT)-related proteins in mammals, *Drosophila*, and Dictyostelium. J Biol Chem 277:32253–32257
2. Greenberg AS, Egan JJ, Wek SA, Garty NB, Blanchette-Mackie EJ, Londos C 1991 Perilipin, a major hormonally regulated adipocyte-specific phosphoprotein associated with the periphery of lipid storage droplets. J Biol Chem 266:11341–11346
3. Greenberg AS, Egan JJ, Wek SA, Moos Jr MC, Londos C, Kimmel AR 1993 Isolation of cDNAs for perilipins A and B: sequence and expression of lipid droplet-associated proteins of adipocytes. Proc Natl Acad Sci USA 90:12035–12039
4. Blanchette-Mackie EJ, Dwyer NK, Barber T, Coxey RA, Takeda T, Rondinone CM, Theodorakis JL, Greenberg AS, Londos C 1995 Perilipin is located on the surface layer of intracellular lipid droplets in adipocytes. J Lipid Res 36:1211–1226
5. Servetnick DA, Brasaemle DL, Gruia-Gray J, Kimmel AR, Wolff J, Londos C 1995 Perilipins are associated with cholesteryl ester droplets in steroidogenic adrenal cortical and Leydig cells. J Biol Chem 270:16970–16973
6. Lu X, Gruia-Gray J, Copeland NG, Gilbert DJ, Jenkins NA, Londos C, Kimmel AR 2001 The murine perilipin gene: the lipid droplet-associated perilipins derive from tissue-specific, mRNA splice variants and define a gene family of ancient origin. Mamm Genome 12:741–749
7. Brasaemle DL, Rubin B, Harten IA, Gruia-Gray J, Kimmel AR, Londos C 2000 Perilipin A increases triacylglycerol storage by decreasing the rate of triacylglycerol hydrolysis. J Biol Chem 275:38486–38493
8. Sztalryd C, Xu G, Dorward H, Tansey JT, Contreras JA, Kimmel AR, Londos C 2003 Perilipin A is essential for the translocation of hormone-sensitive lipase during lipolytic activation. J Cell Biol 161:1093–1103
9. Tansey JT, Huml AM, Vogt R, Davis KE, Jones JM, Fraser KA, Brasaemle DL, Kimmel AR, Londos C 2003 Functional studies on native and mutated forms of perilipins. A role in protein kinase A-mediated lipolysis of triacylglycerols. J Biol Chem 278:8401–8406
10. Spiegelman BM, Flier JS 1996 Adipogenesis and obesity: rounding out the big picture. Cell 87:377–389
11. Okuno A, Tamemoto H, Tobe K, Ueki K, Mori Y, Iwamoto K, Umesono K, Akanuma Y, Fujiwara T, Horikoshi H, Yazaki Y, Kadowaki T 1998 Troglitazone increases the number of small adipocytes without the change of white adipose tissue mass in obese Zucker rats. J Clin Invest 101:1354–1361
12. Kubota N, Terauchi Y, Miki H, Tamemoto H, Yamauchi T, Komeda K, Satoh S, Nakano R, Ishii C, Sugiyama T, Eto K, Tsubamoto Y, Okuno A, Murakami K, Sekihara H, Hasegawa G, Naito M, Toyoshima Y, Tanaka S, Shiota K, Kitamura T, Fujita T, Ezaki O, Aizawa S, Kadowaki T 1999 PPAR γ mediates high-fat diet-induced adipocyte hypertrophy and insulin resistance. Mol Cell 4:597–609
13. Rosenbaum SE, Greenberg AS 1998 The short- and long-term effects of tumor necrosis factor-α and BRL 49653 on peroxisome proliferator-activated receptor (PPAR)γ2 gene expression and other adipocyte genes. Mol Endocrinol 12:1150–1160
14. Souza SC, Yamamoto MT, Franciosa MD, Lien P, Greenberg AS 1998 BRL 49653 blocks the lipolytic actions of tumor necrosis factor-α: a potential new insulin-sensitizing mechanism for thiazolidinediones. Diabetes 47:691–695
15. Tamori Y, Masugi J, Nishino N, Kasuga M 2002 Role of peroxisome proliferator-activated receptor-γ in maintenance of the characteristics of mature 3T3-L1 adipocytes. Diabetes 51:2045–2055
16. Sambrook J, Fritsch F, Maniatis T 1989 Molecular cloning: a laboratory manual. Cold Spring Harbor, NY: Cold Spring Harbor Laboratory Press; 3.2–16.67
17. Sasai Y, Kageyama R, Tagawa Y, Shigemoto R, Nakanishi S 1992 Two mammalian helix-loop-helix factors structurally related to *Drosophila* hairy and Enhancer of split. Genes Dev 6:2620–2634
18. Frohnert BI, Hui TY, Bernlohr DA 1999 Identification of a functional peroxisome proliferator-responsive element in the murine fatty acid transport protein gene. J Biol Chem 274:3970–3977
19. Tontonoz P, Hu E, Graves RA, Budavari AI, Spiegelman BM 1994 mPPARγ2: tissue-specific regulator of an adipocyte enhancer. Genes Dev 8:1224–1234
20. Teboul L, Febbraio M, Gaillard D, Amri EZ, Silverstein R, Grimaldi PA 2001 Structural and functional characterization of the mouse fatty acid translocase promoter: activation during adipose differentiation. Biochem J 360:305–312
21. Schoonjans K, Watanabe M, Suzuki H, Mahfoudi A, Krey G, Wahli W, Grimaldi P, Staels B, Yamamoto T, Auwerx J 1995 Induction of the acyl-coenzyme A synthetase gene by fibrates and fatty acids is mediated by a peroxisome proliferator response element in the C promoter. J Biol Chem 270:19269–19276
22. Kliewer SA, Forman BM, Blumberg B, Ong ES, Borgmeyer U, Mangelsdorf DJ, Umesono K, Evans RM 1994 Differential expression and activation of a family of murine peroxisome proliferator-activated receptors. Proc Natl Acad Sci USA 1994 91:7355–7359
23. Tansey JT, Sztalryd C, Gruia-Gray J, Roush DL, Zee JV, Gavrilova O, Reitman ML, Deng CX, Li C, Kimmel AR, Londos C 2001 Perilipin ablation results in a lean mouse with aberrant adipocyte lipolysis, enhanced leptin production, and resistance to diet-induced obesity. Proc Natl Acad Sci USA 98:6494–6499
24. Martinez-Botas J, Anderson JB, Tessier D, Lapillonne A, Chang BH, Quast MJ, Gorenstein D, Chen KH, Chan L 2000 Absence of perilipin results in leanness and reverses obesity in Lepr (db/db) mice. Nat Genet 26:474–479
25. Yamauchi T, Waki H, Kamon J, Murakami K, Motojima K, Komeda K, Miki H, Kubota N, Terauchi Y, Tsuchida A, Tsuboyama-Kasaoka N, Yamauchi N, Ide T, Hori W, Kato S, Fukayama M, Akanuma Y, Ezaki O, Itai A, Nagai R, Kimura S, Tobe K, Kagechika H, Shudo K, Kadowaki T 2001 Inhibition of RXR and PPARγ ameliorates diet-induced obesity and type 2 diabetes. J Clin Invest 108:1001–1013
26. Yamauchi T, Kamon J, Ito Y, Tsuchida A, Yokomizo T, Kita S, Sugiyama T, Miyagishi M, Hara K, Tsunoda M, Murakami K, Ohteki T, Uchida S, Takekawa S, Waki H, Tsuno NH, Shibata Y, Terauchi Y, Froguel P, Tobe K, Koyasu S, Taira K, Kitamura T, Shimizu T, Nagai R, Kadowaki T 2003 Cloning of adiponectin receptors that mediate antidiabetic metabolic effects. Nature 423:762–769
27. Yamauchi T, Kamon J, Waki H, Imai Y, Shimozawa N, Hioki K, Uchida S, Ito Y, Takakuwa K, Matsui J, Takata M, Eto K, Terauchi Y, Komeda K, Tsunoda M, Murakami K, Ohnishi Y, Naitoh T, Yamamura K, Ueyama Y, Froguel P, Kimura S, Nagai R, Kadowaki T 2003 Globular adiponectin protected ob/ob mice from diabetes and ApoE-deficient mice from atherosclerosis. J Biol Chem 278:2461–2468
28. Wang YX, Lee CH, Tiep S, Yu RT, Ham J, Kang H, Evans RM 2003 Peroxisome-proliferator-activated receptor δ activates fat metabolism to prevent obesity. Cell 113:159–170
29. Shi Y, Hon M, Evans RM 2002 The peroxisome proliferator-activated receptor δ, an integrator of transcriptional repression and nuclear receptor signaling. Proc Natl Acad Sci USA 99:2613–2618
30. Nishiu J, Tanaka T, Nakamura Y 1998 Isolation and chromosomal mapping of the human homolog of perilipin (PLIN), a rat adipose tissue-specific gene, by differential display method. Genomics 48:254–257
31. Sears IB, MacGinnitie MA, Kovacs LG, Graves RA 1996 Differentiation-dependent expression of the brown adipocyte uncoupling protein gene: regulation by peroxisome proliferator-activated receptor γ. Mol Cell Biol 16:3410–3419

Endocrinology is published monthly by The Endocrine Society (http://www.endo-society.org), the foremost professional society serving the endocrine community.

Nicked β_2-glycoprotein I: a marker of cerebral infarct and a novel role in the negative feedback pathway of extrinsic fibrinolysis

Shinsuke Yasuda, Tatsuya Atsumi, Masahiro Ieko, Eiji Matsuura, Kazuko Kobayashi, Junko Inagaki, Hisao Kato, Hideyuki Tanaka, Minoru Yamakado, Minoru Akino, Hisatoshi Saitou, Yoshiharu Amasaki, Satoshi Jodo, Olga Amengual, and Takao Koike

β_2-Glycoprotein I (β_2-GPI) is proteolytically cleaved by plasmin in domain V (nicked β_2-GPI), being unable to bind to phospholipids. This cleavage may occur in vivo and elevated plasma levels of nicked β_2-GPI were detected in patients with massive plasmin generation and fibrinolysis turnover. In this study, we report higher prevalence of elevated ratio of nicked β_2-GPI against total β_2-GPI in patients with ischemic stroke (63%) and healthy subjects with lacunar infarct (27%) when compared to healthy subjects with normal findings on magnetic resonance imaging (8%), suggesting that nicked β_2-GPI might have a physiologic role beyond that of its parent molecule in patients with thrombosis. Several inhibitors of extrinsic fibrinolysis are known, but a negative feedback regulator has not been yet documented. We demonstrate that nicked β_2-GPI binds to Glu-plasminogen with K_D of 0.37×10^{-6} M, presumably mediated by the interaction between the fifth domain of nicked β_2-GPI and the fifth kringle domain of Glu-plasminogen. Nicked β_2-GPI also suppressed plasmin generation up to 70% in the presence of tissue plasminogen activator, plasminogen, and fibrin. Intact β_2-GPI lacks these properties. These data suggest that β_2-GPI/plasmin-nicked β_2-GPI controls extrinsic fibrinolysis via a negative feedback pathway loop. (Blood. 2004; 103:3766-3772)

© 2004 by The American Society of Hematology

Introduction

β_2-Glycoprotein I (β_2-GPI), also known as apolipoprotein H, is a phospholipid-binding plasma protein. Phospholipid-bound β_2-GPI is one of the major target antigens for antiphospholipid antibodies[1-3] present in patients with antiphospholipid syndrome (APS), an autoimmune disorder characterized by arterial/venous thrombosis and pregnancy morbidity.[4] β_2-GPI has 5 homologous short consensus repeats, designated as domains I to V. Domains of β_2-GPI structurally resemble each other, except that domain V has an extra C-terminal loop and a positively charged lysine cluster. In 1993, Hunt et al[5] reported that β_2-GPI is proteolytically cleaved between Lys317 and Thr318 in domain V (nicked β_2-GPI), being unable to bind to phospholipids. This cleavage is generated by factor Xa or by plasmin, with plasmin being more effective.[6]

A large number of reports have detailed the in vitro properties of β_2-GPI as a natural anticoagulant/procoagulant regulator by inhibiting phospholipid-dependent reactions, such as prothrombinase and tenase activity on platelets or phospholipid vesicles,[7,8] factor XII activation,[9] and anticoagulant activity of activated protein C.[10,11] Apart from specific hemostatic functions, β_2-GPI activates lipoprotein lipase,[12] lowers the triglyceride level,[13] binds to oxidized low-density lipoprotein to prevent the progression of atherosclerosis,[14] and binds to nonself particles or apoptotic bodies to allow their clearance.[15-17] Little attention has been given to the functions of the nicked form of β_2-GPI because its phospholipid-binding activity was thought to exert the physiologic or pathologic functions of β_2-GPI.

Fibrinolytic reactions involve the formation of plasmin from the zymogen plasminogen and the hydrolytic cleavage of fibrin to fibrin degradation products by plasmin. Plasminogen, a 92-kDa glycoprotein, is present in plasma at a concentration of approximately 2 μM.[18] Plasminogen consists of 7 domains: one N-terminal peptide, 5 kringle domains bearing a lysine-binding site (LBS) with the capacity to bind fibrin as well as antifibrinolytic proteins carrying lysine, and one serine protease domain.[19] Plasmin conversion from plasminogen by tissue plasminogen activator (tPA) is a key event in extrinsic fibrinolysis for the thrombolysis against intravascular blood clots. Plasmin is one of the most potent enzymes and has a variety of biologic activities; thus, the regulation of plasmin generation and activity is important to maintain the homeostatic balance in vivo. In particular, an excess of fibrinolytic activity can lead to life-threatening bleeding events. Physiologic inhibitors of extrinsic fibrinolysis include α_2-antiplasmin (α_2-AP)[20] and plasminogen activator inhibitor 1 (PAI-1).[21] These inhibitors regulate fibrinolysis through different mechanisms.

Nicked β_2-GPI has been identified by sandwich enzyme-linked immunosorbent assay (ELISA) in plasma of patients with disseminated intravascular coagulation (DIC)[22] or leukemia,[23] both conditions characterized by massive thrombin generation and fibrinolytic

From the Department of Medicine II, Hokkaido University Graduate School of Medicine, Sapporo, Japan; Department of Internal Medicine, School of Dentistry, Health Sciences University of Hokkaido, Ishikari-Tobetsu, Hokkaido, Japan; Department of Cell Chemistry, Institute of Molecular and Cellular Biology, Okayama University Medical School, Okayama, Japan; National Cardiovascular Center Research Institute, Osaka, Japan; Narita R&D Center, Iatron laboratories Inc, Mito, Chiba, Japan; Department of Medicine, Mitsui Memorial Hospital, Tokyo, Japan; Department of Neurosurgery, Azabu Neurosurgical Hospital, Sapporo, Japan.

Submitted August 7, 2003; accepted January 5, 2004. Prepublished online as *Blood* First Edition Paper, January 15, 2004; DOI 10.1182/blood-2003-08-2712.

Supported in part by grants from the Japanese Ministry of Health, Labour and Welfare, by those from the Japanese Ministry of Education, Culture, Sports, Science and Technology, and by the Sankyo Foundation of Life Science.

Reprints: Tatsuya Atsumi, Department of Medicine II, Hokkaido University Graduate School of Medicine, N15, W7, Kita-ku, Sapporo 060-8638, Japan; e-mail: at3tat@med.hokudai.ac.jp.

The publication costs of this article were defrayed in part by page charge payment. Therefore, and solely to indicate this fact, this article is hereby marked "advertisement" in accordance with 18 U.S.C. section 1734.

© 2004 by The American Society of Hematology

turnover. To investigate the biologic and clinical significance of nicked β_2-GPI in a disease characterized by a lower level of thrombin generation and fibrin turnover than DIC, we evaluated the cleavage ratio of β_2-GPI in plasma of patients with ischemic stroke and the results are presented herein. Further, we investigated the role of nicked β_2-GPI in extrinsic fibrinolysis and demonstrate for the first time that nicked β_2-GPI binds to plasminogen. We also describe the inhibitory effect of nicked β_2-GPI on the fibrin surface where plasminogen is proteolytically activated into plasmin. Because β_2-GPI may be cleaved in vivo by plasmin during thrombus formation and thrombolysis, these phenomena represent a novel negative feedback loop in extrinsic fibrinolysis where β_2-GPI plays a key role.

Patients, materials, and methods

Study patients

The study population comprised 62 patients with history of ischemic stroke diagnosed by magnetic resonance imaging (MRI) performed at the time of admission to the Azabu Neurosurgical Hospital (female-to-male ratio, 12:50; mean age, 68 ± 9 years). Blood samples were obtained from the patients at least 6 months after their last occlusive event.

We also investigated 130 age- and sex-matched apparently healthy subjects with no history of cerebral infarct who consented to join the study. All subjects underwent a cerebral MRI at the Neuroradiology Department at Mitsui Memorial Hospital and images were analyzed by an experienced neuroradiologist. According to the MRI findings the healthy subjects were divided into 2 groups: 52 with lacunar infarcts (female-to-male ratio, 20:32; mean age 67 ± 9 years) and 78 without any abnormality (female-to-male ratio, 26:52; mean age, 66 ± 6 years). Blood sampling was performed at the same time of the MRI scan. All the patients and healthy volunteers provided informed consent according to Declaration of Helsinki principles.

Blood collection

Venous blood was collected in tubes containing one-tenth volume of 0.105 M sodium citrate and was centrifuged immediately at 4°C. Plasma samples were depleted of platelets by filtration then stored at −70°C until use.

Materials

Monoclonal antibodies. To measure the plasma levels of nicked or total β_2-GPI, we used 2 monoclonal antibodies, 1 monoclonal anti-nicked β_2-GPI antibody (NGPI-60) that specifically reacts against nicked β_2-GPI and the other monoclonal anti-β_2-GPI antibody (NGPI-23) that equally reacts with nicked and intact β_2-GPI.[23]

An IgG mouse monoclonal antihuman β_2-GPI antibody directed to domain III of human β_2-GPI (Cof-22) was used for the purification of nicked β_2-GPI and evaluation of the binding of nicked β_2-GPI to immobilized Glu-plasminogen.[24] Cleavage of β_2-GPI by plasmin did not affect the binding of Cof-22 to β_2-GPI because the epitope of Cof-22 antibody on β_2-GPI molecule resides on domain III (data not shown).

Antihuman plasminogen antibodies directed to kringles 1 to 3 or against kringle 4 were obtained from American Diagnostica (Greenwich, CT).

Proteins. β_2-GPI was purified from human plasma, as described.[25] Nicked β_2-GPI was prepared as reported[26] with slight modifications that included an additional purification step; β_2-GPI was treated with human plasmin (Calbiochem Novabiochem, La Jolla, CA) at 37°C for 3 hours, at a molar ratio of β_2-GPI/plasmin of 8:1. Plasmin-treated β_2-GPI was first purified on a Cof 22–Sepharose column and subsequently on a heparin-Sepharose column. The heparin nonbinding fraction was collected and further purified by ion-exchange chromatography using Mono-Q column (Pharmacia Biotech, Uppsala, Sweden). Purified β_2-GPI was reduced using 2-mercaptoethanol and subjected to sodium dodecyl sulfate–polyacrylamide gel electrophoresis (SDS-PAGE), appearing as a single band smaller than that of the intact one (data not shown).

The domain V–deleted mutant protein (domains I-IV) of β_2-GPI was expressed using a baculovirus system as reported.[24] This mutant β_2-GPI does not include the cleavage site for plasmin.

Glu-plasminogen was purified from the plasma of healthy Japanese donors using chromatography on lysine-Sepharose 4B (Pharmacia Biotech) and diethylaminoethyl (DEAE) Sephadex A-50 (Pharmacia Biotech). Plasminogen kringles 1 to 3 fragment, plasminogen kringle 4 fragment, and mini-plasminogen, which consists of the kringle 5 and serine protease domain of plasminogen, were obtained from Technoclone (Vienna, Austria). Recombinant tPA (2-chain, Duteplase) was obtained from Sumitomo Pharmaceutical (Osaka, Japan). ε-Aminocaproic acid (EACA) was purchased from Sigma Chemical (St Louis, MO).

Methods

Measurement of plasma levels of nicked β_2-GPI. Plasma levels of nicked β_2-GPI were determined by a sandwich ELISA as previously described with slight modifications.[23] Briefly, polystyrene microtiter plates were coated with 100 μL monoclonal anti–nicked β_2-GPI antibody (NGPI-60) in 50 mM Tris (trishydroxymethylaminomethane)–HCL, pH 7.5, containing 0.15 M NaCl and incubated overnight at 4°C. Wells were washed 3 times with 0.5 M NaCl containing 0.05% Tween 20 and 100 μL citrated plasma samples diluted 5-fold in 20 mM Tris-HCl, pH 7.5, containing 0.5 M NaCl and 0.05% Tween 20 (sample buffer) were added. After 2 hours of incubation at room temperature and washing 3 times, 100 μL biotinylated $F(ab')_2$ fragment of monoclonal anti-β_2-GPI (NGPI-23; 2 μg/mL) was added to each well, followed by 1 hour of incubation. Then, 100 μL alkaline phosphatase (ALP)–conjugated streptavidin (Zymed, San Francisco, CA) at a 1:1000 dilution in sample buffer was added to each well. After another 1 hour of incubation and 3 times washing, 200 μL substrate (1 mg/mL p-nitrophenylphosphate disodium [Sigma Chemical] in 1 M diethanolamine buffer [pH 9.8]) was added. Optical density (OD) was read at 492 nm with reference at 620 nm using an ELISA plate reader. The plasma levels of nicked β_2-GPI were determined from a standard curve constructed with citrated plasma spiked with known amounts of purified nicked β_2-GPI.

Measurement of plasma levels of total β_2-GPI. Plasma levels of total β_2-GPI were determined by a sandwich ELISA using F(ab') fragment of NGPI-23 as the capture antibody and biotinylated antihuman β_2-GPI rabbit IgG as the tag antibody as previously reported.[23] Plasma samples of 50 μL (8000-fold diluted) were added to the wells containing the immobilized antibody. The ALP-conjugated streptavidin (Zymed) was then added and bound ALP was determined as described ("Measurement of plasma levels of nicked β_2-GPI"). The amounts of total β_2-GPI in plasma were calculated from a calibration curve constructed with known amounts of purified β_2-GPI. A nicked β_2-GPI ratio was calculated in all samples using the formula: (plasma nicked β_2-GPI/plasma total β_2-GPI) × 1000.

Other laboratory investigations. The same plasma samples were tested for thrombin-antithrombin (TAT) complexes, plasmin-antiplasmin (plasmin inhibitor) complex (PPI), and D-dimers (DDs) by latex agglutination assay using commercial kits LPIAACE TAT, LPIAACE PPI, LPIAACE D-D dimer (Dia-Iatron, Tokyo, Japan), according to the manufacturer's instructions.

ELISA for binding of intact or nicked β_2-GPI to plasminogen. The binding of nicked or intact β_2-GPI was investigated by ELISA. Fifty microliters of Glu-plasminogen (10 μg/mL) in phosphate-buffered saline (PBS), pH 7.4, was distributed in each well of a Sumilon Type S microtiter ELISA plate (Sumitomo Bakelite, Tokyo, Japan) and incubated overnight at 4°C. After washing twice with PBS and blocking with 2% gelatin-PBS for 1 hour at 37°C, 50 μL of serial dilutions of intact or nicked β_2-GPI in 1% bovine serum albumin (Sigma Chemical)–PBS (1% BSA-PBS) were placed in each well. Plates were incubated for 1 hour at room temperature and washed 3 times with PBS containing 0.05% Tween 20 (PBS-Tween), then 50 μL/well Cof-22 (100 ng/mL) in 1% BSA-PBS was distributed. After incubation and washing as above, 50 μL/well of ALP-conjugated anti-mouse IgG (Sigma Chemical), diluted 1:2000 in 1% BSA-PBS, was put into each well, followed by incubation. Substrate (100 μL) was distributed after washing 4 times with PBS-Tween and incubated. OD was read at 405 nm with reference at 620 nm.